



HAL
open science

Spatio-temporal trends of hydrological components: the case of the Tafna basin (northwestern Algeria)

Amina Mami, Djilali Yebdri, Sabine Sauvage, Mélanie Raimonet, José Miguel SANCHEZ PEREZ

► **To cite this version:**

Amina Mami, Djilali Yebdri, Sabine Sauvage, Mélanie Raimonet, José Miguel SANCHEZ PEREZ. Spatio-temporal trends of hydrological components: the case of the Tafna basin (northwestern Algeria). *Journal of Water and Climate Change*, 2021, 12, pp.2948 - 2976. 10.2166/wcc.2021.242 . hal-03830393

HAL Id: hal-03830393

<https://hal.science/hal-03830393>

Submitted on 26 Oct 2022

HAL is a multi-disciplinary open access archive for the deposit and dissemination of scientific research documents, whether they are published or not. The documents may come from teaching and research institutions in France or abroad, or from public or private research centers.

L'archive ouverte pluridisciplinaire **HAL**, est destinée au dépôt et à la diffusion de documents scientifiques de niveau recherche, publiés ou non, émanant des établissements d'enseignement et de recherche français ou étrangers, des laboratoires publics ou privés.

Spatio-temporal trends of hydrological components: the case of the Tafna basin (northwestern Algeria)

Amina Mami, Djilali Yebdri, Sabine Sauvage, Mélanie Raimonet and José Miguel

ABSTRACT

Climate change is expected to increase in the future in the Mediterranean region, including Algeria. The Tafna basin, vulnerable to drought, is one of the most important catchments ensuring water self-sufficiency in northwestern Algeria. The objective of this study is to estimate the evolution of hydrological components of the Tafna basin, throughout 2020–2099, compared to the period 1981–2000. The SWAT model (Soil and Water Assessment Tool), calibrated and validated on the Tafna basin with good Nash at the outlet 0.82, is applied to analyze the spatial and temporal evolution of hydrological components over the basin throughout 2020–2099. The application is produced using a precipitation and temperature minimum/maximum of an ensemble of climate model outputs obtained from a combination of eight global climate models and two regional climate models of the Coordinated Regional Climate Downscaling Experiment project. The results of this study show that the decrease of precipitation in January, on average -25% , ranged between -5% and -44% in the future period. This diminution affects all of the water components and fluxes of a watershed, namely, in descending order of impact: the river discharge causing a decrease -36% , the soil water available -31% , the evapotranspiration -30% , and the lateral flow -29% .

Key words | CORDEX-Africa, hydrology, precipitation, SWAT, Tafna basin

HIGHLIGHTS

- Impact of climate change in northwestern Africa;
- Modeling a semi-arid watershed using SWAT model;
- Evaluation of the influence of decline rainfall on the hydrological cycle;
- The use of RCMs of Cordex project, domain Africa;
- Investigation of climatic trends at monthly scale.

INTRODUCTION

The impacts of climate change have interested scientists in northern Africa since the last decades of the 20th century, when the decrease of precipitation and the increase of temperature were noticed (Arnell *et al.* 2003; Zettam *et al.*

This is an Open Access article distributed under the terms of the Creative Commons Attribution Licence (CC BY-NC-ND 4.0), which permits copying and redistribution for non-commercial purposes with no derivatives, provided the original work is properly cited (<http://creativecommons.org/licenses/by-nc-nd/4.0/>).

doi: 10.2166/wcc.2021.242

Amina Mami (corresponding author)

Djilali Yebdri

LGTE, University of Sciences and Technology Oran
Mohamed Boudiaf,
Oran,
Algeria
E-mail: mami.amina89@yahoo.fr

Sabine Sauvage

Mélanie Raimonet

José Miguel

Laboratoire Ecologie fonctionnelle et
Environnement,
UMR 5245, Université de Toulouse, CNRS, INPT,
UPS,
Toulouse,
France

2017; Mami *et al.* 2021). The decrease of precipitation detected in northwestern Algeria is estimated as -25% in the 1970s compared to the period of 1950–2000 (Arnell 1999; Knippertz *et al.* 2003), predicting the rise of the vulnerability of this semi-arid region as regards water stress. The decrease of precipitation affects water resources, in which a decline of flow is already noted as -60% in the 1970s compared to the period 1930–1998 (Meddi *et al.* 2010; Taibi *et al.* 2017).

One of the domains affected by climate change is water resources, induced by the decrease of precipitation and the increase in temperature. This may have an impact on drinking water, and industrial and agricultural activities, leading to serious droughts in some regions, such as the southern region of the Mediterranean basin (Solomon et al. 2007; Schilling et al. 2012; AR5 Climate Change 2013: 5; Jacob et al. 2014; Price 2017; Brouziyne et al. 2018; Zeroual et al. 2018). The level of water resource stress in Algeria, assessed by Arnell (1999), is medium (−20 to −40% of use/water resource ratio) in the last decade of the 20th century, and becomes high, exceeding 40%, for the future period (2025–2085). The Tafna basin, situated in northwestern Algeria, is one of the most important catchments ensuring the water self-sufficiency in this region (Zettam et al. 2017). The Tafna basin was impacted by the decline of the water resource during the 1970s (Meddi & Hubert 2003) and a decrease of this resource is estimated in the Tafna basin over the 21st century (Mami et al. 2021).

The northwestern region of Africa is characterized by a wet winter and a dry summer (Yebdri et al. 2007; Zettam et al. 2017; Gevaert et al. 2018). In the future period, Brouziyne et al. (2018) mention that the months mostly affected by climate change are January for precipitation and July for temperature in the R'dom watershed (Morocco), near to the Tafna basin and with similar climate characteristics.

The diminution of precipitation affects the water cycle, composed of runoff, soil water availability, and evapotranspiration. In northern Africa, the decrease of runoff, river discharge, and precipitation is underlined mainly in winter (Arnell 1999; Brouziyne et al. 2018; Grusson et al. 2018; Naumann et al. 2018; Zeroual et al. 2018; Burek et al. 2019). Groundwater is also impacted, but it is difficult to separate the role of climate change and local anthropogenic interferences (Kundzewicz & Doll 2009; Taylor et al. 2011; Green 2016; Grusson et al. 2018). All of these components are connected and change in one of them could interfere with another one (Grusson et al. 2018), as evapotranspiration and soil water availability are strongly linked (Manabe et al. 2004; Calanca et al. 2006; Jung et al. 2010; Verrot & Destouni 2016; Grusson et al. 2018).

Recent studies use regional climate models (RCMs) to investigate climate change, in northwest Africa (e.g., CNRM-CM5-RCA4, IPSL-IPSL-CM5A-MR-CCLM4-8-17,

ICHEC-EC-EARTH-DMI, etc.) from the Coordinated Regional Climate Downscaling Experiment (CORDEX) project's Africa domain by Mami et al. (2021) and Zeroual et al. (2018) for the Algerian part, Europe by Brouziyne et al. (2018), and Seifennasr et al. (2016) for the Moroccan part. The project ENSEMBLE, European domain, is also used by Taibi et al. (2017). The decrease of precipitation indicated in these studies is around −10 to −40% under the Representative Concentration Pathways (RCPs) 4.5 and 8.5, respectively. The temperature is also affected by climate change, with an increase of 1.3 °C on average at an annual scale within 2050 (Brouziyne et al. 2018). Also, the flow is not spared from climate change and is expected to decrease by −40% in the Mediterranean region within 2099 (AR4 2007).

As suggested by Zettam et al. (2017) and Todini (2007), the hydrological models are useful for diverse objectives, such as for decision-makers, namely, water resource managers, urban planners, and administrations (Noori & Kalin 2016). Different distributed physically based models can simulate temporal and spatial variations of hydrological processes and work out the influence of land use impacts (Lin et al. 2015). Among these models are Hydrological Infiltration Capacity (VIC) (Liang et al. 1994), Institute of Hydrology Distributed Model (IHDM) (Beven et al. 1987), WATFLOOD (Kouwen et al. 1993), and Système hydrologique Européen (SHE) (Abbott et al. 1986).

The Soil and Water Assessment Tool (SWAT) (Arnold et al. 1998) is used for a supplementary function to assess: agricultural management practices (Moriassi et al. 2011), hydrology and sediment transfer (Arnold et al. 2012; Gassman et al. 2014; Zettam et al. 2017, 2020), and evaluating the impacts of climate change (Singh & Gosain 2011; Grusson et al. 2018). Numerous studies use SWAT in semi-arid watersheds, such as in Southern Australia (Shrestha et al. 2016), Spain (Molina-Navarro et al. 2014), Brazil (Santos et al. 2019), and North Africa (Bouraoui et al. 2005; Yebdri et al. 2007; Sellami et al. 2016; Zettam et al. 2017), and others for assessing climate change (Nerantzaki et al. 2015; Yanjie et al. 2015; Jin et al. 2016; Brouziyne et al. 2018; Grusson et al. 2018; Saddique et al. 2019; Yuan 2019; Mami et al. 2021).

Our study aims to detect the impact of climate change over the future period (2020–2099) on the hydrological components of the Tafna basin, using hydrological modeling forced with climate model outputs (precipitation and

temperature maximum/minimum) of the CORDEX-Africa initiative. The approach developed in this paper is considered for future climate throughout 2020–2099. This application is proceeded by the SWAT model to analyze the spatial and temporal evolution of hydrological water balance over the Tafna basin, for hydrological SWAT components (precipitation, river discharge, runoff, subsurface flow, soil water content, evapotranspiration, etc.). The trends are presented in this study with two Representation Concentration Pathway (RCP) scenarios (4.5 and 8.5) on a monthly scale.

MATERIALS AND METHODS

Study area

The transboundary Tafna watershed is situated in the northwest of Algeria, and 30% of its surface area is situated in the northeastern part of Morocco (Yebdri *et al.* 2007). It

represents one of the most important basins of the Oranie-chott-cherGUI region according to the classification of the Agence Nationale des Ressources Hydriques (1981) (ANRH: National Water Resources Agency). The area of the Tafna basin is 7,245 km² and flows into the Mediterranean Sea near Beni-saf city (Figure 1). The elevation of the basin is from 0 to 1,800 m a.s.l., situated between the Mediterranean Sea and the Sahara desert.

The climate of the Tafna basin is semi-arid, characterized by wet winters, and hot and dry summers. The annual mean temperature varies between 11 °C in winter and 28 °C in summer, and annual precipitation ranges from 220 to 673 mm/yr during 1981–2000 (Agence Nationale des Ressources Hydriques 1981; Mami *et al.* 2021). The monthly precipitation is almost negligible in summer (from June to September), not exceeding 10 mm, and varies between 20 and 60 mm in winter (Figure 2). While the maximum monthly temperature reaches 33 °C in summer, the minimum monthly temperature in winter can drop to 2 °C (Figure 2).

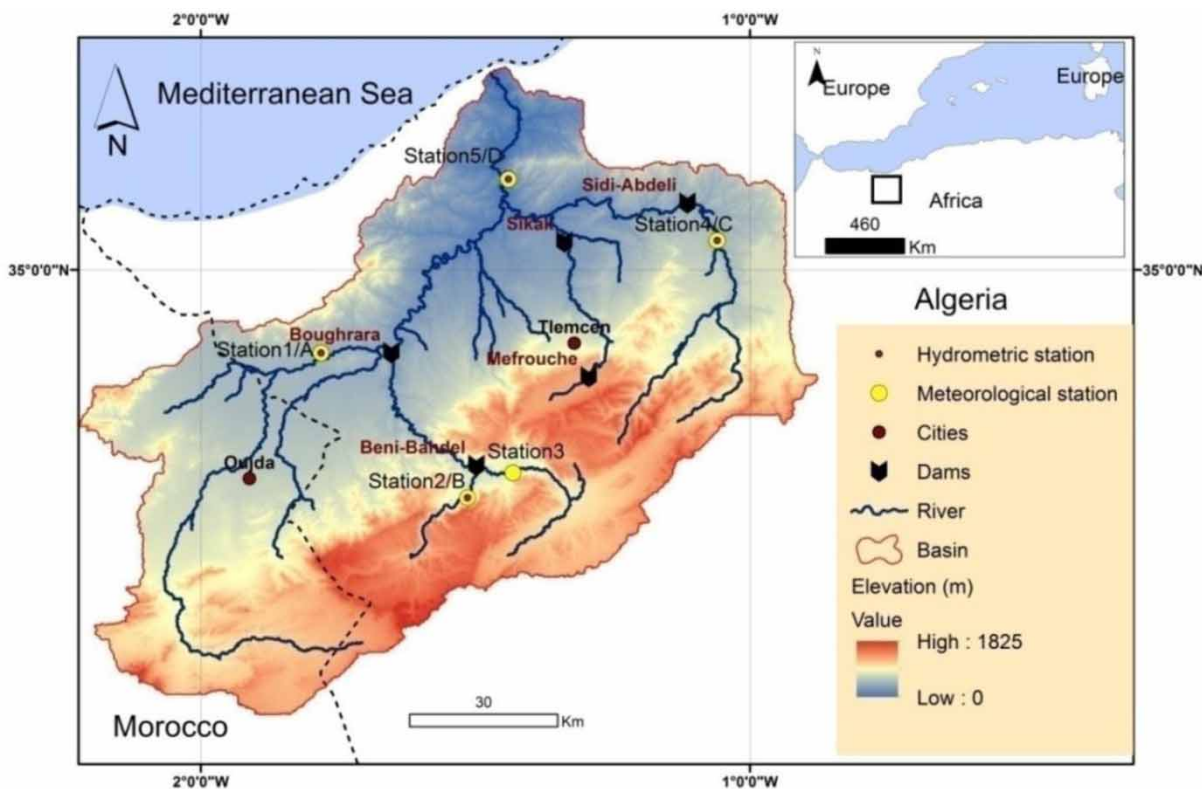


Figure 1 | Location of the Tafna catchment, with (station (number/letter): meteorological/hydrological stations) (Mami *et al.* 2021).

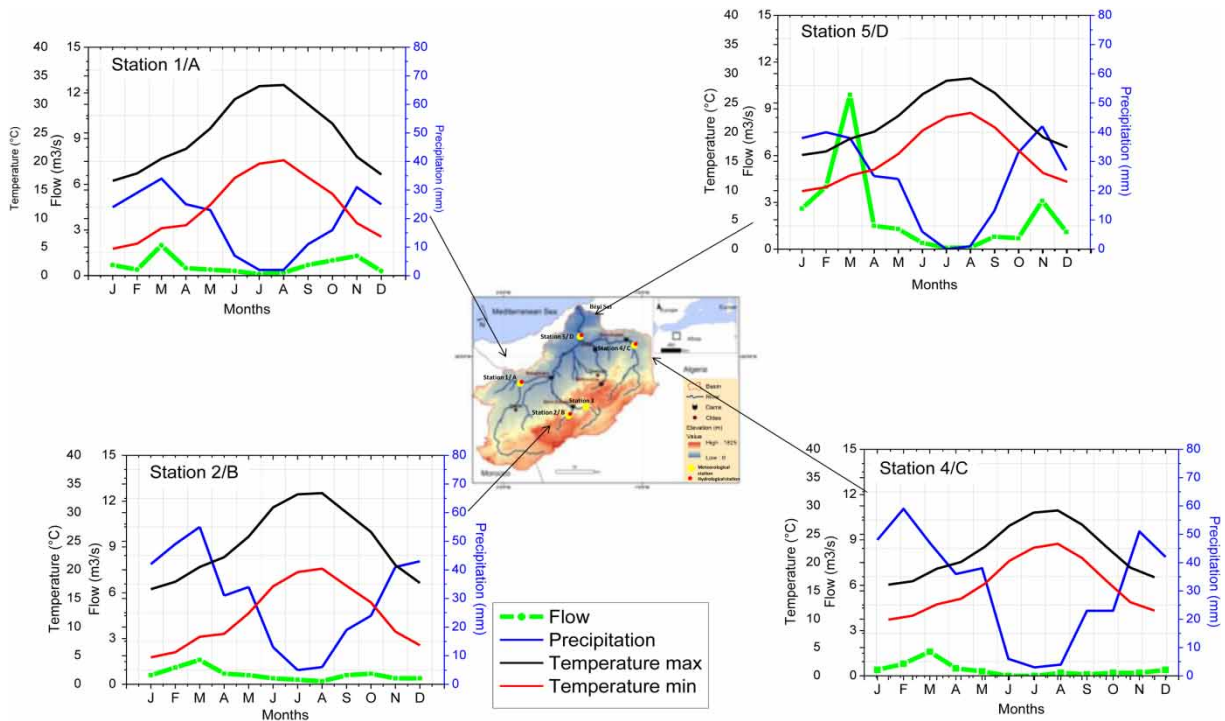


Figure 2 | Observed monthly mean flow, precipitation, and maximum/minimum temperature for the period 1981–2000 (ANRH 1981).

The Tafna basin includes five dams: Beni Bahdel (built in 1952 across Oued Khmis and Oued Tafna, with a capacity of 63 Mm³), Mefrouche (1963, O. Meffrouche, 15 Mm³), Sidi Abdely (1988, O. Isser, 110 Mm³), Boughrara (1998, O. Mouilah, 177 Mm³), and Sikak (2005, O. Sikkak, 27 Mm³) with a total capacity of 392 Mm³ (Yebdri 2006; ANBT 2015; Mami et al. 2021) intended for the supply of drinking, industrial and irrigation water for neighboring cities. The flow recorded during the studied period (1981–2000) ranges on average between 0 and 10 m³/s for 170 km of river course (Agence Nationale des Ressources Hydriques 1981).

Regional climate model outputs

Ten climate model outputs of precipitation and air temperature from the CORDEX-Africa project (CORDEX Data Search | CORDEX | ESGF-CoG n.d.) are used in this work (Table 1). Two regional climate models (RCM) are employed and forced with eight different global climate models (GCM): the regional climate model CCLM4-8-17 is forced by EC-EARTH and CNRM-CM5, and RCA4 is forced by

Table 1 | List of climate model outputs used in this study (the domain used is Africa with 50 km of resolution)

Regional climate model (RCM)	Global climate model (GCM)	Historical	RCP	
			4.5	8.5
CCLM4-8-17	EC-EARTH	X	X	X
	CNRM-CM5	X	X	X
RCA4	EC-EARTH	X	X	X
	CNRM-CM5	X	X	X
	IPSL-CM5A-MR	X	X	X
	CCCma-CanESM2	X	X	X
	MIROC5	X	X	X
	MPI-ESM-LR	X	X	X
	NCC-NorESM1	X	X	X
	NOAA/GFDL-ESM2M	X	X	X

Details about GCM and RCM models can be found on the CORDEX website (<https://esg-dn1.nsc.liu.se/search/cordex/>).

EC-EARTH, CNRM-CM5, IPSL-CM5A-MR, CCCma-CanESM2, MIROC, MPI-ESM-LR, NCC-NorESM1, and NOAA/GFDL-ESM2M. The grid spacing of RCMs used in this study is 0.44 degrees (50 km of resolution) under two RCPs, 4.5 and 8.5. The reference period is the period with available observations (1981–2000). These climate

model (CM) outputs are extracted and bias-corrected by the CMhyd software (Rathjens et al. 2016), using the distribution mapping method for correcting both precipitation and air temperature. The performance of bias correction used in this study is detailed in a previous study (Mami et al. 2021).

Hydrological modeling and datasets

The SWAT model is made for hydrological modeling of watersheds varying from a few hundred to multiple thousands of square kilometers (Zettam et al. 2017), which is the case with the Tafna basin (7,245 km²). The application is divided into two steps: (1) the conception, calibration, and validation of the SWAT model for the Tafna basin detailed in a previous study (Mami et al. 2021) during the period (1981–2000), and (2) the run of the model forced with a set of bias-corrected RCMs' outputs to evaluate the future climatic and hydrologic components' evolutions (2020–2099).

The following inputs are introduced into the SWAT model to produce the hydrological modeling and calibrate the Tafna project. The digital elevation model (DEM) is introduced into SWAT with a resolution of 30 × 30 m to define the basin, the river channel network, and delineate the basin into sub-basins (in this study, 33 sub-basins result from the delineation of the SWAT model for an area of 7,245 km²). The maps soil and land-use are inserted to characterize, joined to DEM, each hydrological response unit (HRU). The slope classes are derived from DEM (four classes: 5%, 15%, 30%, and higher than 30%). More details are shown in a previous paper (Mami et al. 2021).

The meteorological and hydrometric datasets (Figure 1 and Table 2), situated in the Tafna basin, are collected by the National Agency of the Meteorology of Algeria. The daily precipitation and minimum/maximum temperature

datasets from five weather stations (Figure 1) are introduced into the SWAT model, on a daily scale, to run the modeling of the Tafna project for 1981–2010. However, for the calibration and validation of the model, the measured discharge from four hydrometric stations, obtained from the ANRH, are used on a monthly scale for the period 1981–2010 (three years for warm-up, from 1984 to 1995 for calibration, and from 1996 to 2010 for validation). Additional information about datasets can be found in Table 2.

The hydrological modeling is proceeded by the application of the SWAT hydrological model with version 2012 and ArcGIS interface (version 10.2). The Tafna hydrological model is calibrated and validated at the monthly scale for the past periods 1981–1995 and 1996–2010, respectively (including a three-year warm-up period in the calibration period) (Table 3). The calibration and validation are performed using SWAT-CUP (SWAT calibration and uncertainty procedures) (Yebdri et al. 2007; Abbaspour 2007; Zettam et al. 2017, 2020) with SUFI-2 (Sequential Uncertainty Fitting 2) algorithm (Abbaspour et al. 2004). The correlation between measured and simulated discharge observed and simulated is from satisfactory (station C with NSE = 0.54) to very good (station D with NSE = 0.84). The correlation at station A is only unsatisfactory during the validation step (NSE = 0.21). A more detailed description of the performance of calibration and validation of the SWAT model in the case of the Tafna basin can be found in Mami et al. (2021).

Description of SWAT components' calculations

The difference between precipitation and evapotranspiration is the water available for human use and management.

The water cycle components used in this study, namely, surface runoff, subsurface runoff, soil water content, and

Table 2 | Dataset characteristics for SWAT model inputs and discharge for calibration/validation procedures

Data type	Data source	Chronology	Data scale
DEM (digital elevation model)	ASTER global digital elevation model (ASTER Global Digital Elevation Map n.d.)	/	30 m × 30 m
Land use	The European Land Use Agency (Land-Use Map n.d.)	/	1:100,000
Soil	FAO soil (FAO (Harmonized World Soil Database) n.d.)	/	1:1,000,000
Climatic data (1; 2; 3; 4; 5)	National Agency of Meteorology of Algeria	1981–2010	Daily
Hydrometric data (A; B; C; D)	ANRH: Agence Nationale des Ressources Hydriques	1981–2010	monthly

Table 3 | Calibration/validation (with performance rating of the NSE (Nash & Sutcliffe 1970))

Stations	Calibration (1981–1995)				Validation (1996–2010)			
	NSE	R ²	KGE	Performance rating	NSE	R ²	KGE	Performance rating
A	0.61	0.65	0.58	Satisfactory	− 0.30	0.21	0.16	Unsatisfactory
B	0.62	0.69	0.65	Good	0.65	0.71	0.57	Good
C	0.52	0.54	0.4	Satisfactory	0.54	0.58	0.43	Satisfactory
D	0.83	0.84	0.72	Very good	0.66	0.70	0.56	Good

The results of NSE and R² are taken from our previous study (Mami et al. 2021).

evapotranspiration, are computed by the SWAT model as follows.

Surface runoff

In the SWAT model, the runoff computing is effected from the equation of curve number, as follows:

$$Q_{surf} = \frac{(R_{day} - I_a)^2}{(R_{day} - I_a + S)}$$

where Q_{surf} is the accumulated runoff or precipitation excess (mm H₂O), R_{day} is the precipitation depth of the day (mm H₂O), I_a is the initial abstraction which includes surface storage, interception, and infiltration before runoff (mm H₂O), S is the retention parameter (mm H₂O) defined as:

$$S = 25.4 \left(\frac{1000}{CN} - 10 \right)$$

where CN is the curve number of the day, and I_a is commonly approximated as $0.2S$, the equation for Q_{surf} becomes:

$$Q_{surf} = \frac{(R_{day} - 0.2S)^2}{(R_{day} + 0.8S)}$$

Subsurface flow

Lateral flow occurs in the case where the depth is less than 2 meters; by this condition the excess water can be calculated

as follows:

$$SW_{ly, excess} = SW_{ly} - FC_{ly} \text{ if } SW_{ly} > FC_{ly}$$

where $SW_{ly, excess}$ is the drainable volume of water in the soil layer on a given day (mm H₂O), SW_{ly} is the water content of the soil layer on a given day (mm H₂O), FC_{ly} is the water content of the soil layer at field capacity.

The net discharge of hillslope outlet Q_{lat} is given by:

$$Q_{lat} = 0.024 \left(\frac{2 \times SW_{ly, excess} \times K_{sat} \times slp}{\emptyset_d \times L_{hill}} \right)$$

where Q_{lat} is the water discharged from the hillslope outlet (mm H₂O/day), K_{sat} is the saturated hydraulic conductivity (mm/h), slp is the slope (m.m^{−1}) and L_{hill} is the hillslope length (m), and \emptyset_d is the drainable porosity of the soil (mm/mm).

Soil water content

In SWAT, the soil is discretized into several horizons (maximum 10), the number and characteristics of which depend on each type of soil, and are entered by the user. The water content of soils can vary between 0 and a maximum \emptyset_{soil} value when it is saturated. \emptyset_{soil} , therefore, represents porosity. It is expressed as (Grusson 2016) a fraction of the total volume of soil by:

$$\emptyset_{soil} = 1 - \frac{\rho_b}{\rho_s}$$

where \emptyset_{soil} is the soil porosity expressed as a fraction of the

total soil volume, ρb is the bulk density (Mg.m^{-3}), ρs is the density of solid fraction (Mg.m^{-3}).

Evapotranspiration

For the case of the Tafna project, the Hargreaves method is selected to calculate the evapotranspiration:

$$E_t = \frac{E'_0 \times LAI}{3} \text{ for } 0 < LAI \leq 3.0$$

$$E_t = E'_0 \text{ for } LAI > 3.0$$

where E_t is the maximum transpiration on a given day ($\text{mm H}_2\text{O}$), E'_0 is the evapotranspiration adjusted for evaporation on free water in the canopy ($\text{mm H}_2\text{O}$), LAI is the leaf area index. More details are shown in the documentation of Neitsch et al. (2005).

Performance of climate model outputs on the SWAT model

This following application is made for the hydrological SWAT components: precipitation, discharge, runoff, subsurface flow (lateral flow), soil water content, and evapotranspiration.

After calibrating the SWAT model on the Tafna basin, the ten climate model outputs (precipitation and air temperature) are introduced into SWAT to run the model. The SWAT components' outputs using the ten climate models presented in this study are compared to outputs obtained using meteorological observations during the reference period (1981–2000) (Figure 3). This first step allows us to validate the climate model outputs used in this study, and investigate the trends of water cycle components at the Tafna watershed-scale over the future period (2020–2099).

In a second step, the application of the Mann–Kendall test (Mann 1945) is performed for each output forced by the climate model outputs on the two months, January and July, to identify the significant trends over the periods concerned (reference and future). This application precedes the comparison of the future periods (2020–2039, 2040–2059, 2060–2079, and 2080–2099) to the reference period (1981–2000) by estimating the delta existing between the

future periods (every 19 years listed before) and the reference one (1981–2000) (the absolute variation). The delta computed between the projection, of the mean ensemble of the ten climate model outputs, and reference periods are used to investigate the spatial distribution of each water cycle component at the Tafna basin, over the future period, and understand the impact of climate changes in the region at periodic scale (for the periods 2020–2039, 2040–2059, 2060–2079 and 2080–2099).

$$\Delta = (2020 - 2039)_{\text{future period}} - (1981 - 2000)_{\text{reference period}}$$

where Δ is the difference between the variable of the future period and that of the reference period, for each water cycle component (river discharge, precipitation, runoff, lateral flow, soil water content, and evapotranspiration) in mm/year (in mean) for the months January and July. This application is produced for each future period from the first one 2020–2039 to the fourth and last one 2080–2099.

RESULTS

Figure 3 presents the comparison between the SWAT component outputs' simulations (precipitation, evapotranspiration, soil water content, surface flow, and subsurface flow) from the observations and the ten bias-corrected climate model outputs used in this study. This comparison is proceeded by distribution, in the form of boxplots, of each climate model output and observation for the monthly SWAT component outputs, during the reference period (1981–2000). An evaluation of the similarity between SWAT component outputs using ten climate model outputs of CORDEX-Africa shows the concordance of the SWAT component outputs' distribution for the majority of climate model outputs. The similarity between the outputs of the climate models is more suitable in January. That can lead to proceeding with the evaluation of trends at the Tafna watershed-scale over the future period (2020–2099).

Table 4 illustrates the evolution of monthly precipitation from the reference period (1981–2000) to the projected period (divided into four future periods: 2020–2039, 2040–2059, 2060–2079, and 2080–2099). A considerable difference is detectable between the months of January and July.

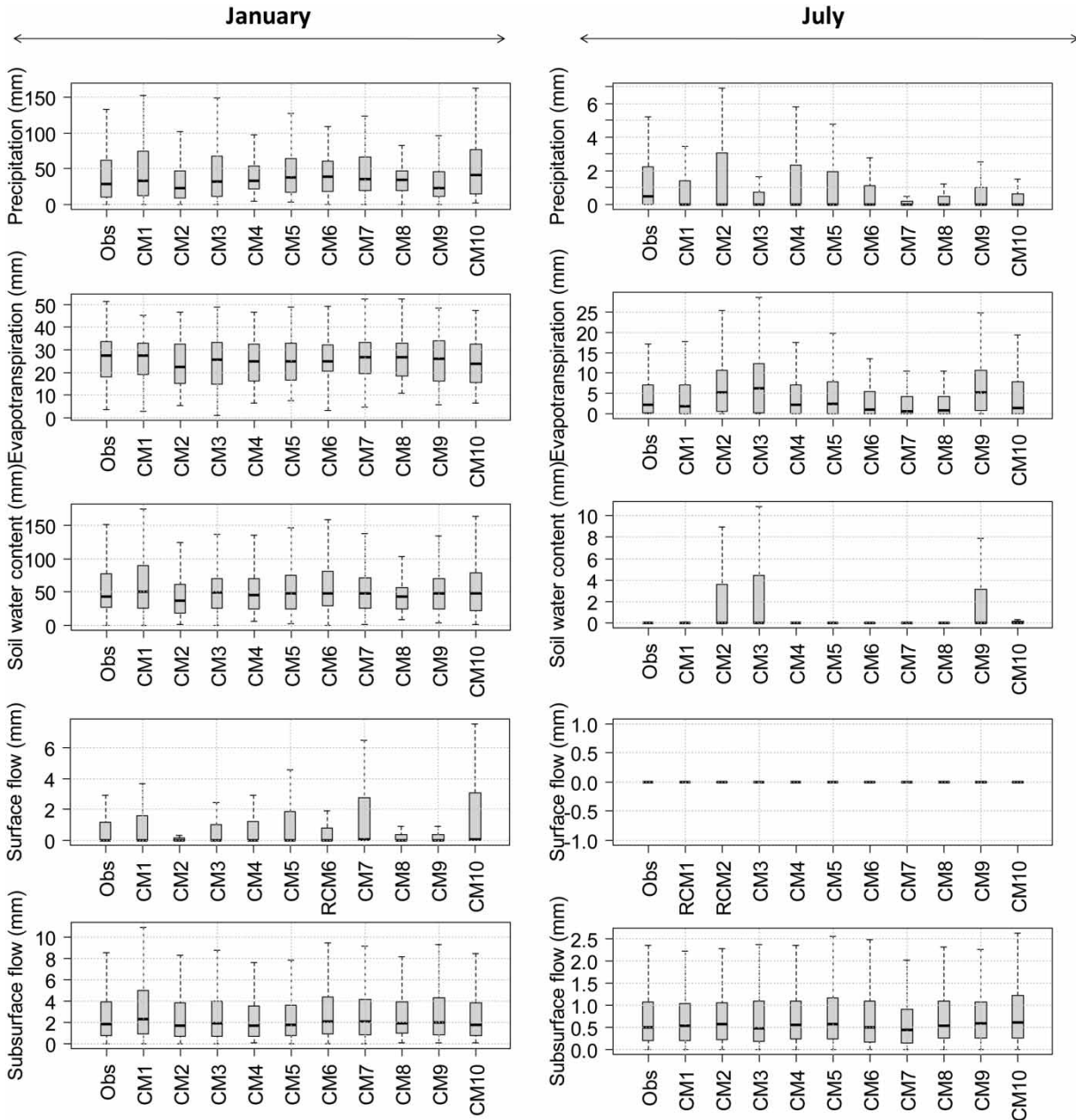


Figure 3 | Comparison between SWAT components' outputs in mm/year of simulations from observation and the ten bias-corrected climate models, of CORDEX-Africa project, at the watershed scale, during the reference period (1981–2000), (CM1: EC-EARTH-CCLM4-8-17, CM2: IPSL-CM5A-MR-RCA4, CM3: CCCma-CanESM2-RCA4, CM4: CNRM-CM5- CCLM4-8-17, CM5: CNRM-CM5-RCA4, CM6: EC-EARTH-RCA4, CM7: MIROC5-RCA4, CM8: MPI-ESM-LR-RCA4, CM9: NCC-NorESM1-RCA4, CM10: NOAA/GFDL-ESM2M-RCA4.

During January, the tendency of precipitation is not clear between the climate models during the studied period, except for the periods 2080–2099, and 2060–2079 and 2080–2099, under RCP 4.5 and 8.5, respectively, that belongs to a significant decrease to 24 mm. The geographic presentation in Figure 4 gives more information about the

tendency of precipitation of the ensemble of climate models over the Tafna basin. In January, the precipitation in the reference period attains 60 mm in the southern and eastern part of the basin, in the future period the decrease appears throughout the period, and seems more important in mountainous areas. However, in July, an increase,

Table 4 | Precipitation trends at the watershed scale for January and July, for the reference period (1981–2000) and the future period (2020–2039, 2040–2059, 2060–2079, and 2080–2099)**Precipitation****1981–2000**

	January				July											
	T		p-value		T		p-value									
Simulated from observation	–		0.9		+		0.7									
EC-EARTH- CCLM4-8-17	+		0.005		–		0.33									
IPSL-CM5A-MR- RCA4	+		0.007		–		0.9									
CCCma-CanESM2- RCA4	+		0.9		–		0.01									
CNRM-CM5- CCLM4-8-17	–		0.004		–		0.37									
CNRM-CM5- RCA4	+		0.9		+		< 0.001									
EC-EARTH- RCA4	+		0.66		+		0.34									
MIROC5- RCA4	–		0.68		–		< 0.001									
MPI-ESM-LR- RCA4	+		< 0.001		–		< 0.001									
NCC-NorESM1- RCA4	+		0.48		+		0.8									
NOAA/GFDL-ESM2M- RCA4	–		< 0.001		–		< 0.001									
RCP 4.5																
	2020–2039				2040–2059				2060–2079				2080–2099			
	January		July		January		July		January		July		January		July	
	T	p-value	T	p-value	T	p-value	T	p-value	T	p-value	T	p-value	T	p-value	T	p-value
EC-EARTH- CCLM4-8-17	+	0.1	–	< 0.001	–	0.003	–	< 0.001	+	0.9	–	< 0.001	–	0.02	–	< 0.001
IPSL-CM5A-MR- RCA4	–	< 0.001	–	0.8	–	0.02	+	< 0.001	+	< 0.001	–	0.01	–	< 0.001	+	< 0.001
CCCma-CanESM2- RCA4	–	0.3	–	< 0.001	+	0.2	+	0.4	–	< 0.001	+	< 0.001	–	0.5	+	< 0.001
CNRM-CM5- CCLM4-8-17	+	0.1	+	< 0.001	+	0.004	–	0.001	+	< 0.001	+	0.2	–	0.06	+	0.2
CNRM-CM5- RCA4	–	< 0.001	+	< 0.001	+	< 0.001	+	0.03	+	< 0.001	+	0.9	–	0.09	–	< 0.001
EC-EARTH- RCA4	+	< 0.001	–	< 0.001	–	< 0.001	–	0.4	+	< 0.001	–	< 0.001	–	< 0.001	–	0.003
MIROC5- RCA4	+	< 0.001	+	0.4	–	< 0.001	+	0.003	+	0.008	–	0.009	–	< 0.001	+	< 0.001
MPI-ESM-LR- RCA4	+	0.005	+	0.5	+	< 0.001	+	< 0.001	–	< 0.001	+	0.004	–	< 0.001	+	0.007
NCC-NorESM1- RCA4	–	< 0.001	–	0.03	+	< 0.001	–	< 0.001	+	0.1	+	< 0.001	–	< 0.001	+	0.0003
NOAA/GFDL-ESM2M- RCA4	–	< 0.001	+	0.1	–	< 0.001	–	0.01	+	0.2	+	0.1	–	< 0.001	–	< 0.001
RCP 8.5																

	2020–2039				2040–2059				2060–2079				2080–2099			
	January		July		January		July		January		July		January		July	
	T	<i>p</i> -value	T	<i>p</i> -value	T	<i>p</i> -value	T	<i>p</i> -value	T	<i>p</i> -value	T	<i>p</i> -value	T	<i>p</i> -value	T	<i>p</i> -value
EC-EARTH- CCLM4-8-17	–	< 0.001	–	< 0.001	+	<u>0.01</u>	–	< 0.001	+	0.7	+	0.9	–	< 0.001	+	< 0.001
IPSL-CM5A-MR- RCA4	–	< 0.001	+	< 0.001	–	< 0.001	–	0.001	+	< 0.001	–	0.4	+	< 0.001	–	< 0.001
CCCma-CanESM2- RCA4	+	< 0.001	–	0.9	+	<u>0.01</u>	–	0.1	–	< 0.001	–	< 0.001	–	0.0001	+	0.7
CNRM-CM5- CCLM4-8-17	+	<u>0.007</u>	–	0.001	+	< 0.001	+	0.003	–	0.6	–	< 0.001	–	< 0.001	+	<u>0.01</u>
CNRM-CM5- RCA4	+	0.4	+	<u>0.07</u>	+	< 0.001	+	0.7	–	< 0.001	+	< 0.001	–	< 0.001	–	0.04
EC-EARTH- RCA4	–	< 0.001	+	0.1	+	0.1	–	< 0.001	–	0.005	–	<u>0.0006</u>	–	<u>0.06</u>	+	<u>0.002</u>
MIROC5- RCA4	+	< 0.001	+	< 0.001	–	< 0.001	–	<u>0.02</u>	–	< 0.001	–	< 0.001	–	< 0.001	–	<u>0.03</u>
MPI-ESM-LR- RCA4	–	< 0.001	+	< 0.001	+	0.2	+	0.001	–	0.0006	–	0.06	+	< 0.001	–	< 0.001
NCC-NorESM1- RCA4	+	0.06	+	< 0.001	–	< 0.001	+	<u>0.03</u>	+	< 0.001	+	< 0.001	–	0.1	+	0.6
NOAA/GFDL-ESM2M- RCA4	+	< 0.001	–	<u>0.006</u>	–	< 0.001	+	< 0.001	–	<u>0.01</u>	–	< 0.001	+	0.1	–	< 0.001

Bold numbers are significant trends (T) considering $\alpha = 0.1$ and underlined numbers considering $\alpha = 0.05$ with the Mann-Kendall test.

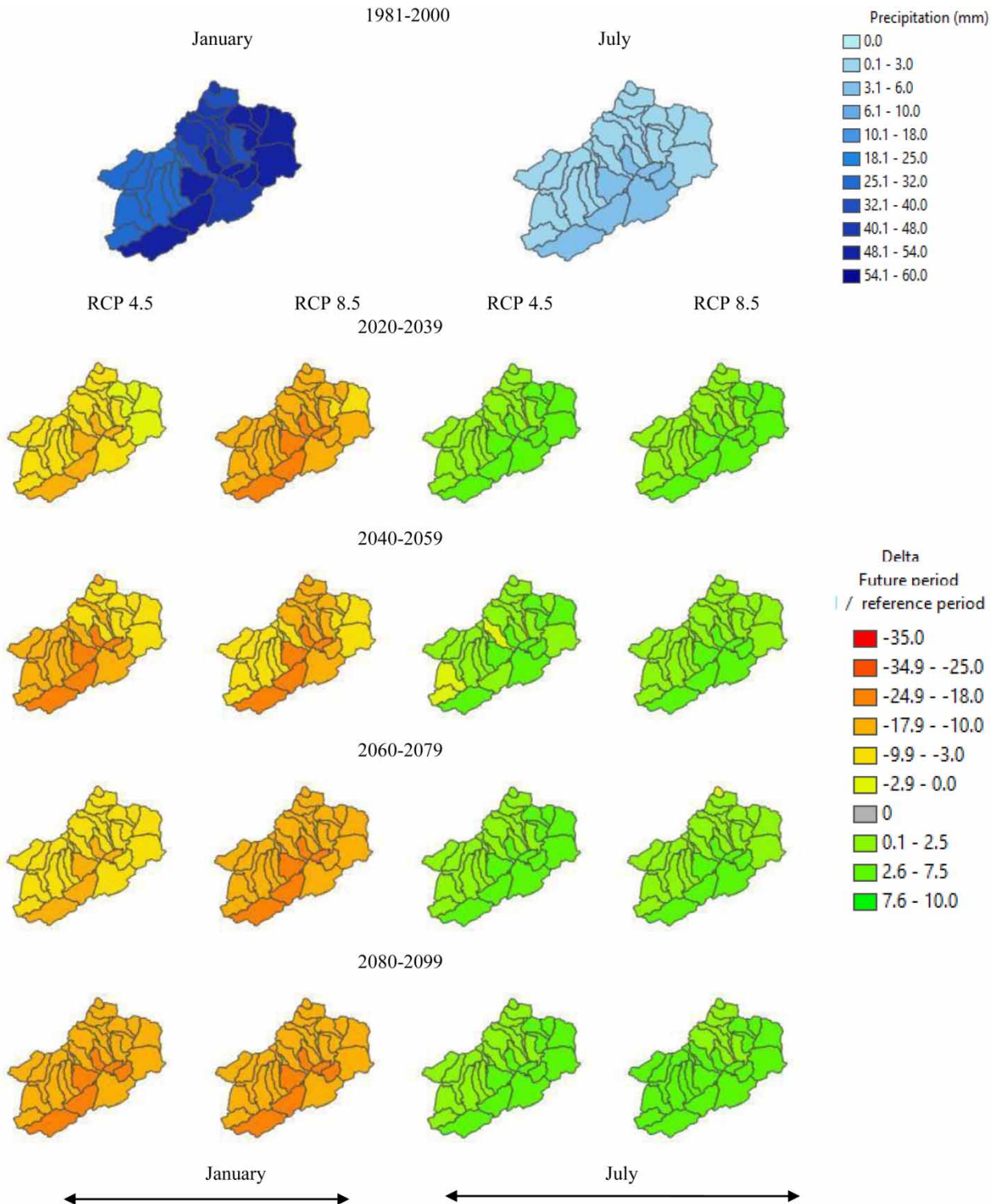


Figure 4 | Total monthly precipitation during the reference period (1981–2000) and absolute variations for the periods (2020–2039, 2040–2059, 2060–2079, and 2080–2099) under RCPs 4.5 and 8.5, for January (left) and July (right).

ranging between 0.1 and 7.5 mm, is distributed over the basin compared to the reference period.

The ratio increase/decrease is balanced while the decrease of discharge appears significant in the periods 2040–2059 and 2080–2099 under RCP 4.5 and the two last periods 2060–2079, 2080–2099 under RCP 8.5 according to the Mann–Kendall test (Table 5). This significant decrease is also marked in Figure 5.

Figure 6 shows the decrease in runoff to be high in January for the periods 2040–2059 and 2080–2099 under RCP 4.5 and 2020–2039, 2060–2079, and 2080–2099 under RCP 8.5. For July the positive delta marked in the basin is negligible, not exceeding 1 mm. For the rest of the future period, the ratio of increase/decrease is balanced between the models (Table 6), and some models give a poor significance of tendency because the p -values are high.

The subsurface flow decreases in the majority of periods for both RCP 4.5 and 8.5, especially in the eastern part of the basin (Figure 7). The results of the Mann–Kendall test shown in Table 7 indicate that the RCMs having a significant decrease of lateral flow surpass those of significant increase, for both January and July over the future period.

A significant decrease in soil water content appears for January, over the future period from 2020–2039 to 2080–2099 (Figure 8). Most models indicate a significant decreasing trend according to the Mann–Kendall test (Table 8).

For July, the reference period presents low rates not exceeding 2 mm, which implies no clear trends for the future period (Table 8), and a minimal delta that is almost negligible (Figure 8).

Concerning evapotranspiration, in January a decrease is marked for the majority of climate models in Table 9 and appears also in Figure 9, which is more pronounced under RCP 8.5 than RCP 4.5. Negative values of the delta are growing from the first period 2020–2039 to the last one 2080–2099. However, for the low values in the reference period for July, the ratio between increase/decrease is inbalanced, and the delta varies between -5 mm and $+3$ mm over the basin.

DISCUSSION

The SWAT model is applied for studying the impact of climate change on hydrological water balance components.

The SWAT model, implanted on the Tafna basin, was calibrated and validated in a previous study Mami *et al.* (2021), during the periods 1981–1995 and 1996–2010, respectively, and the good results of the Nash and the KGE obtained from the calibration/validation (Knoben *et al.* 2019) confirm that multi-sites' calibration is useful for the model to perform well despite the heterogeneity of the watershed (Niraula *et al.* 2012; Jianwen *et al.* 2017; Leta *et al.* 2017; Zettam *et al.* 2017; Grusson *et al.* 2018). The assessment of the hydrological water balance is based on the calibration of the model on river discharge values only because no data are accessible with sufficient temporal and spatial resolution for the other hydrological components. The hydrological water balance resulting from the SWAT project is positively validated against the cartographies of hydrological water balance published by ANRH (2003a, 2003b, 2003c) for the period 1965–2003 and also Meddi *et al.* (2016), regarding precipitation (SWAT values = 314 mm/yr, ANRH values = 250–550 mm/yr), runoff (SWAT values = 19 mm/yr, ANRH values = 10–100 mm/yr), and potential evapotranspiration (SWAT values = 1,260 mm/yr, ANRH values = 900–1,400 mm/yr) (Mami *et al.* 2021). The validation of the SWAT components on the Tafna basin allows us to assess the evolution of these hydrological components in the future. The assessment of the evolution of hydrological water balance components is preceded by the implantation of an ensemble of regional climate models into SWAT, to represent geographically the delta of trends for each SWAT component. These regional climate models are treated and unbiased (Mami *et al.* 2021) by the method of distribution mapping (Block *et al.* 2009; Chen *et al.* 2011; Teutschbein & Seibert 2012, 2013; Fang *et al.* 2015). The validation step of the regional climate models is produced by their comparison to the observed datasets for the reference period (1981–2000). The SWAT components resulting from the ten climate models used in this study give an acceptable representation compared to those resulting from observed datasets. These results confirm the validation of the climate models used to study the tendency of SWAT components on the Tafna basin for the two months of January and July. This validation allows us to use the mean ensemble of the ten outputs obtained, a combination of eight GCMs and two RCMs, to study the climatic and hydrologic trends in the Tafna basin.

Table 5 | Same as Table 4 but for river discharge

Discharge

1981–2000																
	January				July											
	T		P		T		p									
Simulated from observation	+			<u>0.022</u>				–				<u>0.31</u>				
EC-EARTH- CCLM4-8-17	+			<u>0.67</u>				+				< <u>0.001</u>				
IPSL-CM5A-MR- RCA4	+			<u>0.30</u>				–				<u>0.38</u>				
CCCma-CanESM2- RCA4	–			<u>0.14</u>				+				<u>0.06</u>				
CNRM-CM5- CCLM4-8-17	–			<u>0.16</u>				+				<u>0.31</u>				
CNRM-CM5- RCA4	+			< <u>0.001</u>				+				< <u>0.001</u>				
EC-EARTH- RCA4	–			<u>0.007</u>				+				<u>0.57</u>				
MIROC5- RCA4	+			<u>0.56</u>				–				<u>0.18</u>				
MPI-ESM-LR- RCA4	–			<u>0.055</u>				–				< <u>0.001</u>				
NCC-NorESM1- RCA4	+			<u>0.96</u>				+				<u>0.25</u>				
NOAA/GFDL-ESM2M- RCA4	–			< <u>0.001</u>				–				< <u>0.001</u>				
RCP 4.5																
	2020–2039				2040–2059				2060–2079				2080–2099			
	January		July		January		July		January		July		January		July	
	T	p-value	T	p-value												
EC-EARTH- CCLM4-8-17	–	<u>0.5</u>	–	<u>0.8</u>	–	< <u>0.001</u>	–	< <u>0.001</u>	–	<u>0.8</u>	–	<u>0.7</u>	–	<u>0.1</u>	–	< <u>0.001</u>
IPSL-CM5A-MR- RCA4	–	< <u>0.001</u>	–	< <u>0.001</u>	–	< <u>0.001</u>	–	<u>0.003</u>	+	< <u>0.001</u>	+	< <u>0.001</u>	–	< <u>0.001</u>	–	< <u>0.001</u>
CCCma-CanESM2- RCA4	–	< <u>0.001</u>	–	< <u>0.001</u>	+	<u>0.02</u>	+	<u>0.2</u>	–	< <u>0.001</u>	–	<u>0.002</u>	+	<u>0.01</u>	–	<u>0.3</u>
CNRM-CM5- CCLM4-8-17	+	< <u>0.001</u>	+	< <u>0.001</u>	–	<u>0.4</u>	+	<u>0.06</u>	–	< <u>0.001</u>	+	<u>0.01</u>	+	<u>0.6</u>	+	< <u>0.001</u>
CNRM-CM5- RCA4	–	<u>0.3</u>	+	< <u>0.001</u>	–	<u>0.03</u>	+	< <u>0.001</u>	+	< <u>0.001</u>	+	<u>0.3</u>	–	<u>0.4</u>	+	<u>0.1</u>
EC-EARTH- RCA4	+	<u>0.7</u>	–	< <u>0.001</u>	–	< <u>0.001</u>	–	< <u>0.001</u>	–	<u>0.6</u>	+	<u>0.5</u>	–	<u>0.04</u>	–	<u>0.007</u>
MIROC5- RCA4	+	<u>0.4</u>	–	< <u>0.001</u>	–	<u>0.2</u>	+	<u>0.07</u>	+	<u>0.08</u>	–	< <u>0.001</u>	–	<u>0.3</u>	+	<u>0.002</u>
MPI-ESM-LR- RCA4	–	< <u>0.001</u>	+	<u>0.5</u>	+	<u>0.01</u>	+	< <u>0.001</u>	+	<u>0.07</u>	–	<u>0.8</u>	–	<u>0.02</u>	+	< <u>0.001</u>
NCC-NorESM1- RCA4	–	< <u>0.001</u>	+	<u>0.001</u>	–	<u>0.3</u>	+	<u>0.2</u>	–	<u>0.006</u>	–	<u>0.06</u>	+	< <u>0.001</u>	–	< <u>0.001</u>
NOAA/GFDL-ESM2M- RCA4	–	< <u>0.001</u>	+	<u>0.9</u>	–	< <u>0.001</u>	–	< <u>0.001</u>	+	<u>0.1</u>	+	<u>0.1</u>	–	< <u>0.001</u>	–	<u>0.005</u>
RCP 8.5																

	January		July		January		July		January		July	
	2020–2039		2040–2059		2060–2079		2080–2099		2080–2099		2080–2099	
	T	p-value										
EC-EARTH- CCLM4-8-17	+	<u>0.04</u>	+	< <u>0.001</u>	–	<u>0.007</u>	–	< <u>0.001</u>	–	<u>0.4</u>	–	< <u>0.001</u>
IPSL-CM5A-MR- RCA4	–	<u>0.04</u>	–	< <u>0.001</u>	–	< <u>0.001</u>	–	< <u>0.001</u>	+	< <u>0.001</u>	–	< <u>0.001</u>
CCCma-CanESM2- RCA4	+	<u>0.5</u>	+	<u>0.02</u>	–	<u>0.2</u>	+	<u>0.2</u>	+	<u>0.6</u>	–	< <u>0.001</u>
CNRM-CM5- CCLM4-8-17	–	< <u>0.001</u>	–	<u>0.006</u>	+	<u>0.7</u>	+	<u>0.06</u>	+	< <u>0.001</u>	+	<u>0.06</u>
CNRM-CM5- RCA4	–	<u>0.009</u>	–	<u>0.004</u>	+	<u>0.9</u>	+	< <u>0.001</u>	–	<u>0.004</u>	+	< <u>0.001</u>
EC-EARTH- RCA4	+	<u>0.03</u>	+	<u>0.06</u>	+	<u>0.07</u>	–	< <u>0.001</u>	–	< <u>0.001</u>	–	<u>0.01</u>
MIROC5- RCA4	+	<u>0.01</u>	+	< <u>0.001</u>	–	<u>0.003</u>	+	<u>0.07</u>	–	< <u>0.001</u>	+	<u>0.8</u>
MPI-ESM-LR- RCA4	–	< <u>0.001</u>	+	<u>0.1</u>	+	<u>0.4</u>	+	< <u>0.001</u>	–	< <u>0.001</u>	+	<u>0.03</u>
NCC-NorESM1- RCA4	–	<u>0.2</u>	–	<u>0.8</u>	–	< <u>0.001</u>	+	<u>0.2</u>	+	<u>0.02</u>	–	< <u>0.001</u>
NOAA/GFDL-ESM2M- RCA4	+	<u>0.001</u>	+	<u>0.9</u>	–	<u>0.06</u>	–	< <u>0.001</u>	–	<u>0.9</u>	+	<u>0.001</u>

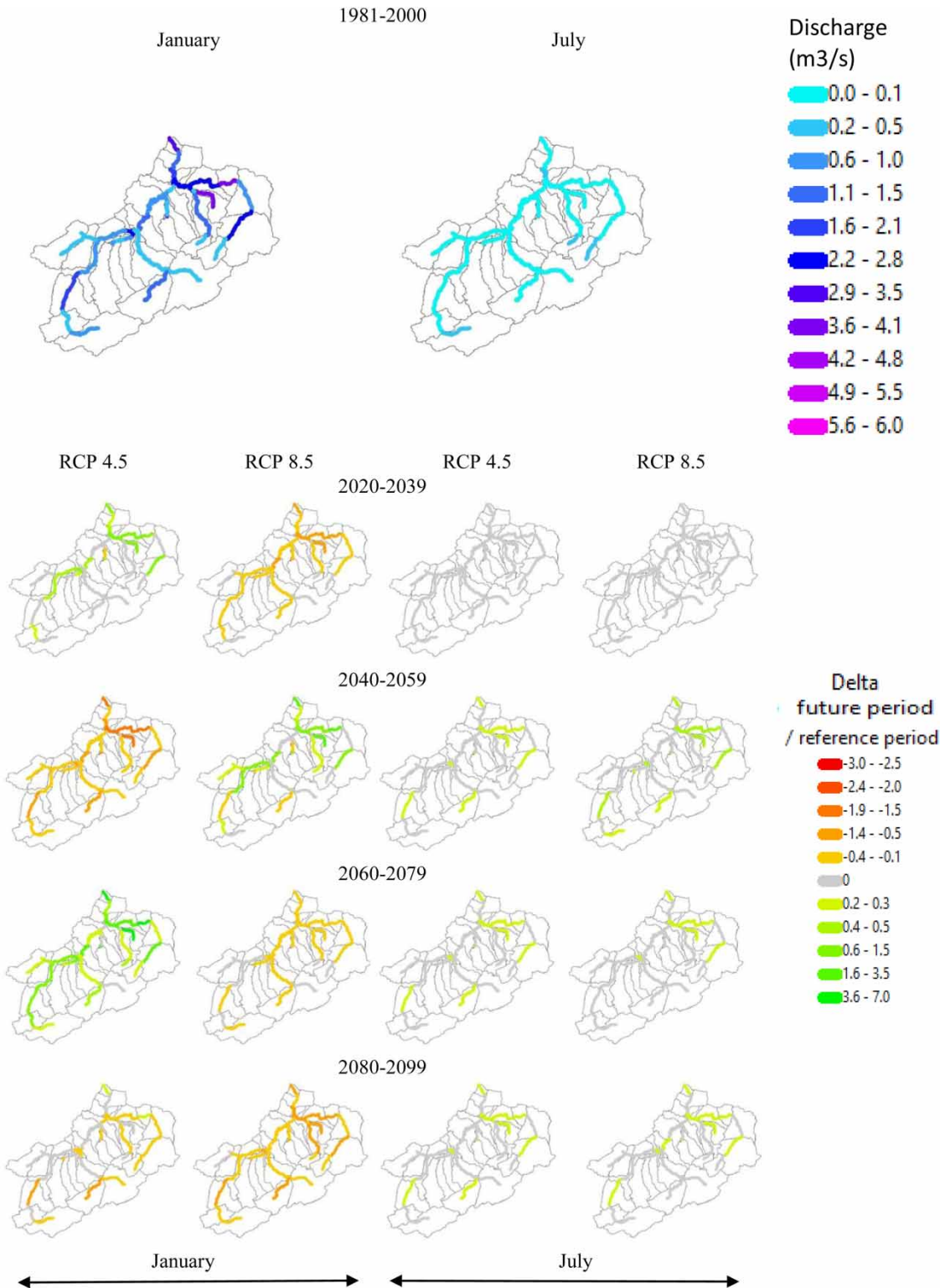


Figure 5 | Mean river discharge during the reference period (1981–2000) and mean absolute variations for the periods (2020–2039, 2040–2059, 2060–2079, and 2080–2099), under RCPs 4.5 and 8.5, compared to 1981–2000 for January and July.

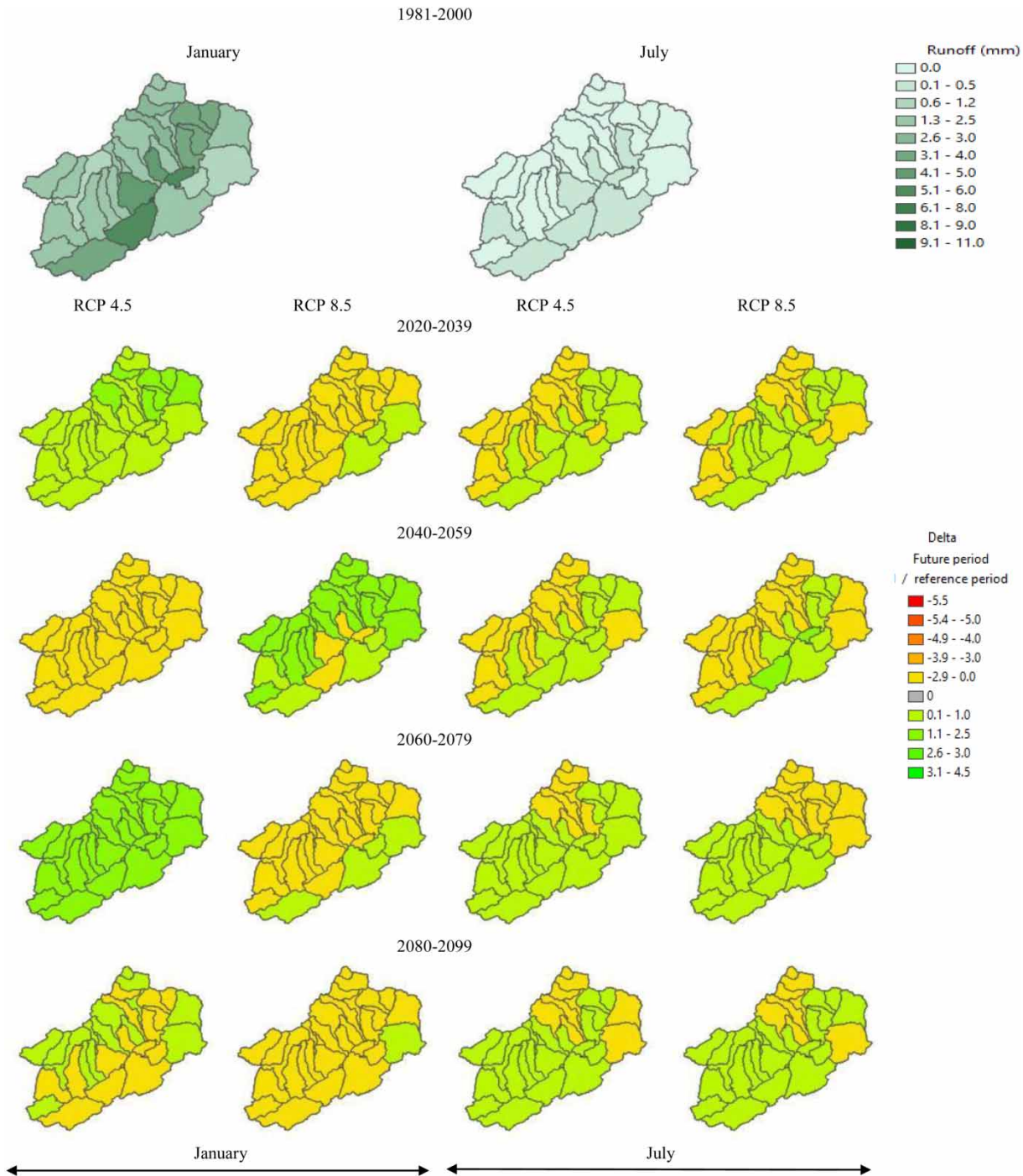


Figure 6 | Runoff during the reference period (1981–2000) and absolute variations for the periods (2020–2039, 2040–2059, 2060–2079, and 2080–2099) at monthly scale for January and July.

The evaluation of the impact of climate change on the water cycle is rare in northwestern Africa and particularly northwestern Algeria, a zone considered vulnerable to climate

change in the last decades of the 20th century (Meddi *et al.* 2010; Taibi *et al.* 2017; Hadour *et al.* 2020). The Tafna basin is characterized by very irregular flow with frequent dry

Table 6 | Same as Table 4 but for surface flow (runoff)**Surface flow (runoff)****1981–2000**

	January				July											
	T	p-value	T	p-value	T	p-value	T	p-value								
Simulated from observation	+				–											
RCP 4.5																
	2020–2039				2040–2059				2060–2079				2080–2099			
	January		July		January		July		January		July		January		July	
	T	p-value	T	p-value												
EC-EARTH- CCLM4-8-17	+	0.2	–	< 0.001	–	< 0.001	–	< 0.001	+	0.47	+	0.66	+	0.058	–	< 0.001
IPSL-CM5A-MR- RCA4	–	< 0.001	–	0.062	–	< 0.001	+	0.001	+	< 0.001	+	< 0.001	–	0.22	+	< 0.001
CCCma-CanESM2- RCA4	–	< 0.001	–	0.68	+	< 0.001	+	0.036	–	0.022	+	< 0.001	+	0.66	+	0.021
CNRM-CM5- CCLM4-8-17	+	0.003	+	< 0.001	+	0.002	–	0.85	+	< 0.001	+	< 0.001	–	0.3	–	0.093
CNRM-CM5- RCA4	–	0.001	+	< 0.001	+	0.023	+	< 0.001	+	< 0.001	–	0.83	+	< 0.001	+	0.38
EC-EARTH- RCA4	+	< 0.001	–	0.027	–	< 0.001	–	0.48	+	< 0.001	–	0.006	–	0.001	+	0.36
MIROC5- RCA4	+	< 0.001	+	< 0.001	–	< 0.001	–	0.63	+	0.0001	–	0.4	–	< 0.001	+	0.01
MPI-ESM-LR- RCA4	–	0.59	+	< 0.001	+	< 0.001	+	< 0.001	+	< 0.001	+	< 0.001	–	< 0.001	+	< 0.001
NCC-NorESM1- RCA4	–	< 0.001	+	< 0.001	+	< 0.001	–	< 0.001	–	0.62	+	0.007	–	0.47	–	0.8
NOAA/GFDL-ESM2M- RCA4	–	< 0.001	–	0.77	–	< 0.001	+	< 0.001	+	< 0.001	–	< 0.001	–	< 0.001	–	< 0.001
RCP 8.5																
	2020–2039				2040–2059				2060–2079				2080–2099			
	January		July		January		July		January		July		January		July	
	T	p-value	T	p-value												
EC-EARTH- CCLM4-8-17	–	0.005	+	< 0.001	+	0.004	–	0.34	–	0.073	+	< 0.001	–	< 0.001	+	0.54
IPSL-CM5A-MR- RCA4	–	< 0.001	+	0.49	–	0.28	+	< 0.001	–	0.72	+	< 0.001	+	< 0.001	+	< 0.001
CCCma-CanESM2- RCA4	+	0.55	+	0.002	+	0.82	+	0.62	–	0.028	–	0.01	–	< 0.001	+	0.52
CNRM-CM5- CCLM4-8-17	+	0.012	–	0.0005	+	< 0.001	–	< 0.001	+	0.58	+	< 0.001	–	< 0.001	+	0.044
CNRM-CM5- RCA4	+	0.49	+	0.052	+	0.01	–	0.011	–	< 0.001	–	0.027	–	< 0.001	+	< 0.001
EC-EARTH- RCA4	–	0.15	+	0.12	+	0.23	–	< 0.001	–	0.28	+	0.097	–	0.001	+	0.61
MIROC5- RCA4	+	< 0.001	+	0.12	–	< 0.001	–	< 0.001	–	< 0.001	+	0.097	–	< 0.001	+	0.61
MPI-ESM-LR- RCA4	–	< 0.001	+	< 0.001	–	0.47	+	0.61	–	< 0.001	+	< 0.001	+	0.0005	–	0.67
NCC-NorESM1- RCA4	+	0.004	+	0.28	–	< 0.001	+	0.61	+	< 0.001	+	0.028	–	0.0008	–	0.061
NOAA/GFDL-ESM2M- RCA4	+	0.007	+	0.1	–	< 0.001	–	0.45	–	< 0.001	+	0.14	–	0.057	–	0.3

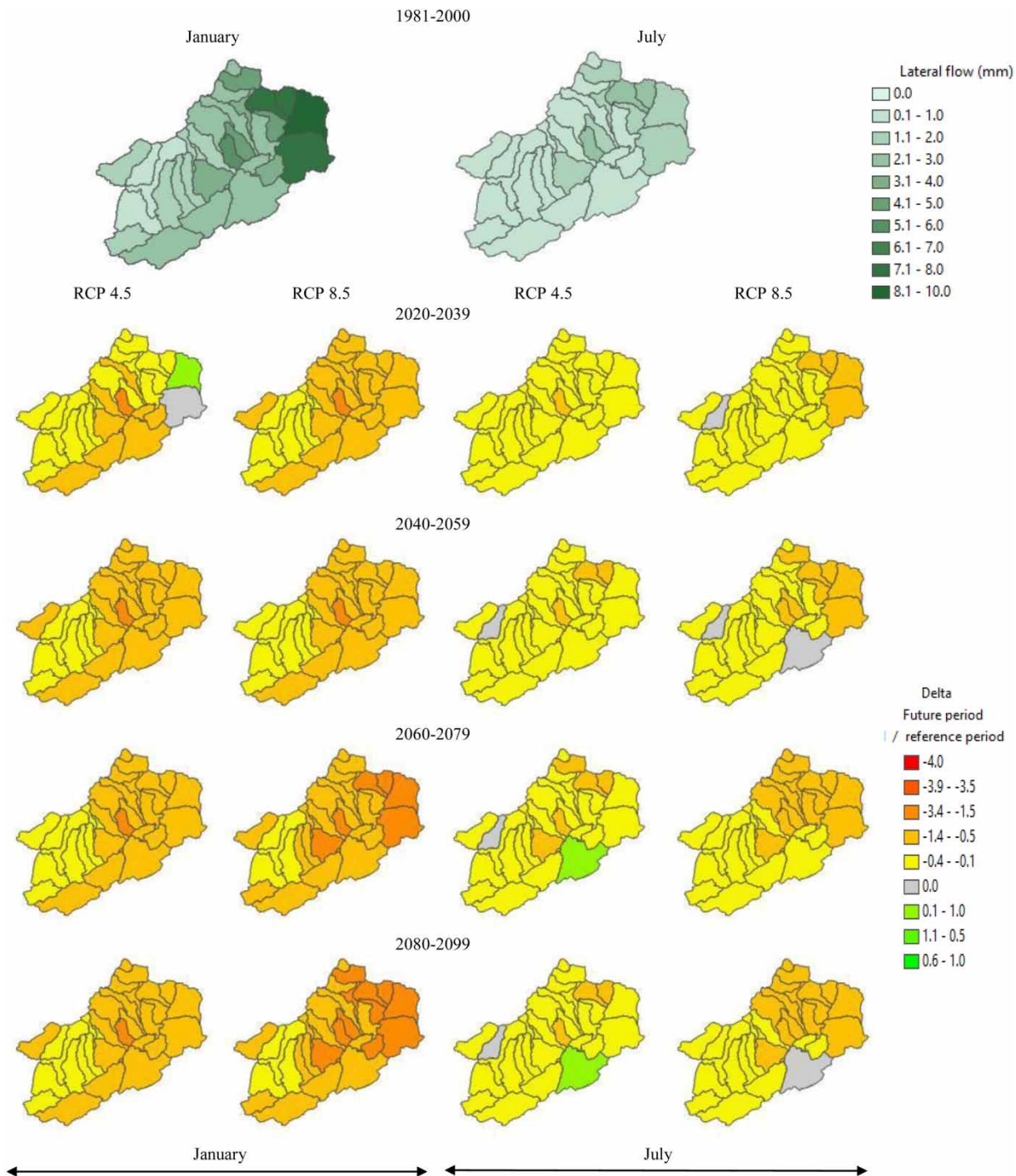


Figure 7 | Subsurface flow (lateral flow) during the reference period (1981–2000) and absolute variations for the periods (2020–2039, 2040–2059, 2060–2079, and 2080–2099) at monthly scale for January and July.

summers, implying very limited permanent reserves (Leta *et al.* 2017; Brouziyne *et al.* 2018). Changes in hydrological components (river discharge, surface flow, subsurface flow, soil

water content, and evapotranspiration) are not obvious for all months but have been highlighted for the months characterized by the most drastic changes in precipitation.

Table 7 | Same as Table 4 but for subsurface flow (lateral flow)**Lateral flow****1981–200**

	January				July											
	T	p-value			T	p-value										
Simulated from observation	+	<u>0.009</u>			–	0.48										
RCP 4.5	2020–2039				2040–2059				2060–2079				2080–2099			
	January		July		January		July		January		July		January		July	
	T	p-value	T	p-value												
EC-EARTH- CCLM4-8-17	–	<u>0.019</u>	+	0.67	–	< <u>0.001</u>	–	< <u>0.001</u>	–	0.33	–	0.13	–	<u>0.006</u>	–	< <u>0.001</u>
IPSL-CM5A-MR- RCA4	–	< <u>0.001</u>	–	< <u>0.001</u>	–	< <u>0.001</u>	–	< <u>0.001</u>	+	0.75	+	<u>0.038</u>	–	< <u>0.001</u>	–	< <u>0.001</u>
CCCma-CanESM2- RCA4	–	< <u>0.001</u>	–	< <u>0.001</u>	+	<u>0.055</u>	+	0.76	–	< <u>0.001</u>	–	<u>0.01</u>	+	<u>0.019</u>	–	0.51
CNRM-CM5- CCLM4-8-17	+	< <u>0.001</u>	+	< <u>0.001</u>	–	0.44	+	0.6	+	< <u>0.001</u>	+	0.77	+	0.41	+	<u>0.013</u>
CNRM-CM5- RCA4	–	0.43	+	< <u>0.001</u>	–	0.033	+	0.42	–	0.04	+	0.52	–	0.063	+	0.98
EC-EARTH- RCA4	–	0.17	–	< <u>0.001</u>	–	< <u>0.001</u>	–	< <u>0.001</u>	+	<u>0.008</u>	–	0.64	–	<u>0.02</u>	–	< <u>0.001</u>
MIROC5- RCA4	–	0.9	–	< <u>0.001</u>	–	< <u>0.001</u>	+	<u>0.051</u>	+	0.5	–	< <u>0.001</u>	–	0.14	+	<u>0.022</u>
MPI-ESM-LR- RCA4	–	< <u>0.001</u>	+	0.42	+	0.28	+	0.16	+	< <u>0.001</u>	–	0.3	–	<u>0.029</u>	+	0.12
NCC-NorESM1- RCA4	–	< <u>0.001</u>	+	0.3	–	<u>0.088</u>	+	0.47	–	<u>0.01</u>	–	<u>0.002</u>	+	<u>0.001</u>	–	< <u>0.001</u>
NOAA/GFDL-ESM2M- RCA4	–	< <u>0.001</u>	–	< <u>0.001</u>	–	< <u>0.001</u>	–	< <u>0.001</u>	+	0.78	+	0.78	–	< <u>0.001</u>	–	< <u>0.001</u>
RCP 8.5	2020–2039				2040–2059				2060–2079				2080–2099			
	January		July		January		July		January		July		January		July	
	T	p-value	T	p-value												
EC-EARTH- CCLM4-8-17	–	0.83	+	< <u>0.001</u>	–	<u>0.091</u>	–	0.52	–	< <u>0.001</u>	–	0.29	–	< <u>0.001</u>	–	<u>0.034</u>
IPSL-CM5A-MR- RCA4	–	<u>0.004</u>	–	< <u>0.001</u>	–	< <u>0.001</u>	–	<u>0.09</u>	–	< <u>0.001</u>	+	<u>0.001</u>	+	0.26	–	< <u>0.001</u>
CCCma-CanESM2- RCA4	+	<u>0.03</u>	+	0.87	–	<u>0.043</u>	–	< <u>0.001</u>	+	0.88	–	< <u>0.001</u>	–	< <u>0.001</u>	–	< <u>0.001</u>
CNRM-CM5- CCLM4-8-17	–	<u>0.004</u>	–	<u>0.059</u>	–	0.392	+	0.18	+	< <u>0.001</u>	+	0.79	–	<u>0.01</u>	–	<u>0.044</u>
CNRM-CM5- RCA4	–	< <u>0.001</u>	–	<u>0.011</u>	–	<u>0.092</u>	+	0.17	–	< <u>0.001</u>	+	<u>0.09</u>	–	< <u>0.001</u>	–	<u>0.004</u>
EC-EARTH- RCA4	+	<u>0.076</u>	+	0.41	–	0.35	+	0.11	–	< <u>0.001</u>	–	< <u>0.001</u>	–	<u>0.009</u>	–	0.56
MIROC5- RCA4	+	0.78	+	< <u>0.001</u>	–	<u>0.002</u>	–	< <u>0.001</u>	–	< <u>0.001</u>	+	0.82	–	< <u>0.001</u>	–	<u>0.002</u>
MPI-ESM-LR- RCA4	–	< <u>0.001</u>	+	< <u>0.001</u>	+	<u>0.001</u>	–	0.38	–	< <u>0.001</u>	–	< <u>0.001</u>	+	<u>0.092</u>	–	< <u>0.001</u>
NCC-NorESM1- RCA4	–	0.49	–	<u>0.039</u>	–	< <u>0.001</u>	–	<u>0.005</u>	+	0.18	–	0.81	–	< <u>0.001</u>	+	<u>0.075</u>
NOAA/GFDL-ESM2M- RCA4	+	<u>0.02</u>	–	0.75	–	<u>0.012</u>	–	0.57	–	0.33	+	0.26	–	<u>0.025</u>	–	< <u>0.001</u>

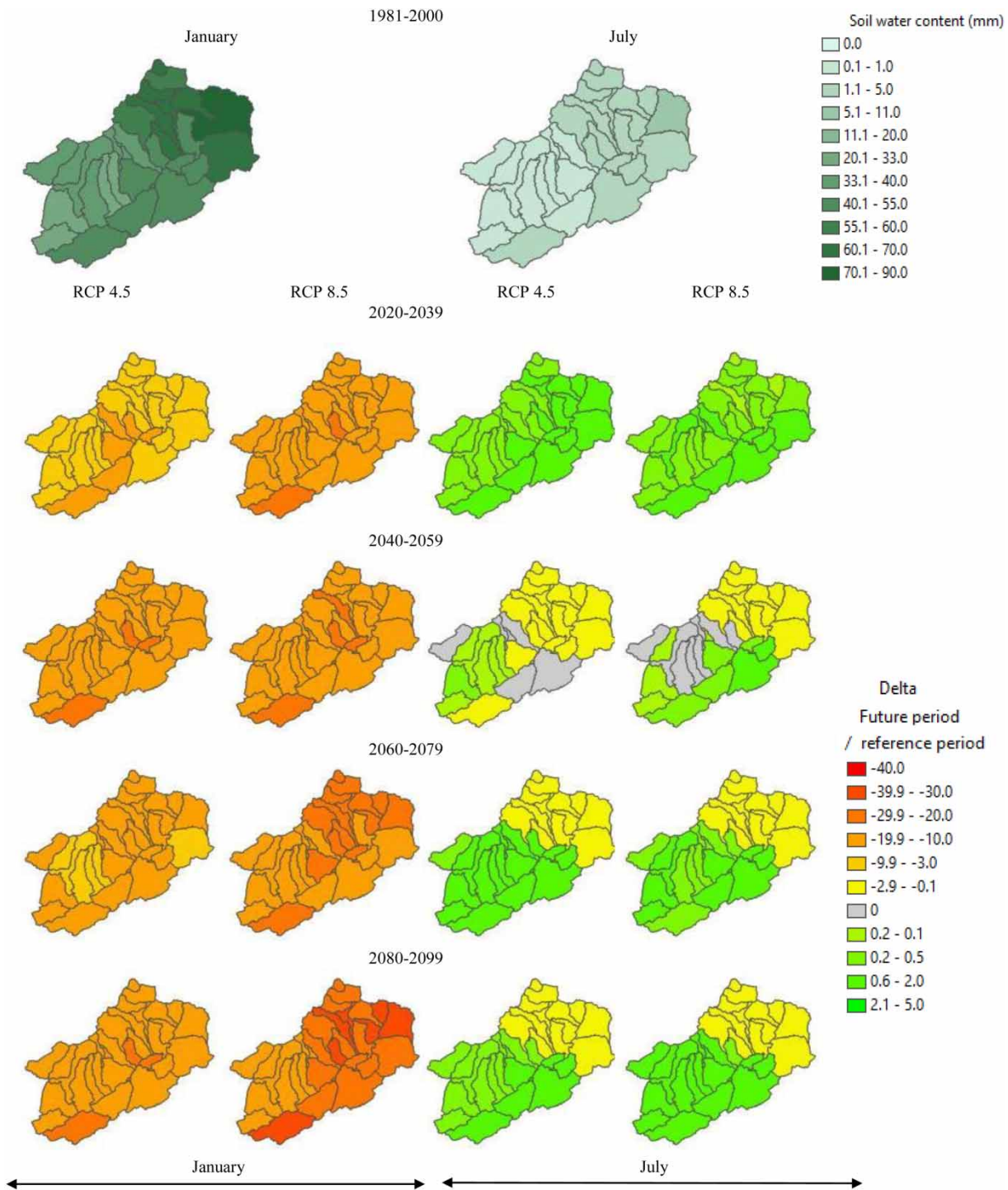


Figure 8 | Soil water content during the reference period (1981–2000) and absolute variations for the periods (2020–2039, 2040–2059, 2060–2079, and 2080–2099) at monthly scale for January and July.

The northwestern region of Africa is characterized by a wet winter and a dry summer (Yebdri *et al.* 2007; Zettam *et al.* 2017; Gevaert *et al.* 2018; Mami *et al.* 2021). In a study

by Xoplaki (2002), the seasonal distribution of precipitation is equivalent to 40% in winter of this region and 10% in summer in the past period.

Table 8 | Same as Table 4 but for soil water content**Soil water content****1981–2000**

	January		July		January		July									
	T	p-value	T	p-value	T	p-value	T	p-value								
Simulated from observation	+		< 0.001		–		0.011									
RCP 4.5	2020–2039		2040–2059		2060–2079		2080–2099									
	January		July		January		July									
	T	p-value	T	p-value	T	p-value	T	p-value								
EC-EARTH- CCLM4-8-17	–	0.016	–	< 0.001	–	< 0.001	–	< 0.001	–	0.7	–	< 0.001	–	0.11	–	0.096
IPSL-CM5A-MR- RCA4	–	< 0.001	–	< 0.001	–	< 0.001	–	0.66	+	0.002	+	0.006	–	< 0.001	–	0.056
CCCma-CanESM2- RCA4	–	0.002	–	< 0.001	+	0.024	+	0.42	–	< 0.001	+	0.001	+	0.016	+	0.057
CNRM-CM5- CCLM4-8-17	+	< 0.001	+	< 0.001	+	0.44	+	0.09	+	< 0.001	+	< 0.001	+	0.38	–	0.18
CNRM-CM5- RCA4	–	0.001	+	0.12	+	0.97	–	0.33	–	0.31	–	0.87	–	< 0.001	+	0.37
EC-EARTH- RCA4	–	0.53	–	< 0.001	–	< 0.001	–	< 0.001	+	0.001	–	0.22	–	0.99	–	0.019
MIROC5- RCA4	+	< 0.001	+	0.21	–	< 0.001	+	0.006	+	0.075	–	< 0.001	–	< 0.001	+	< 0.001
MPI-ESM-LR- RCA4	–	0.0005	–	0.007	+	0.01	+	< 0.001	+	< 0.001	–	0.35	–	< 0.001	+	0.044
NCC-NorESM1- RCA4	–	< 0.001	+	0.1	–	0.009	–	0.002	–	0.035	+	0.31	+	0.01	–	0.28
NOAA/GFDL-ESM2M- RCA4	–	< 0.001	–	0.52	–	< 0.001	+	0.017	–	0.51	–	0.012	–	< 0.001	–	< 0.001
RCP 8.5	2020–2039		2040–2059		2060–2079		2080–2099									
	January		July		January		July									
	T	p-value	T	p-value	T	p-value	T	p-value								
EC-EARTH- CCLM4-8-17	–	< 0.001	+	0.001	+	0.69	–	0.1	–	< 0.001	–	0.011	–	< 0.001	+	0.88
IPSL-CM5A-MR- RCA4	–	< 0.001	–	0.13	–	< 0.001	–	< 0.001	–	< 0.001	+	0.14	–	0.17	–	< 0.001
CCCma-CanESM2- RCA4	+	< 0.001	+	< 0.001	–	0.41	–	0.009	–	0.097	–	0.007	–	< 0.001	–	< 0.001
CNRM-CM5- CCLM4-8-17	–	< 0.001	–	< 0.001	–	0.83	–	0.016	+	< 0.001	+	0.84	–	< 0.001	+	< 0.001
CNRM-CM5- RCA4	–	< 0.001	–	0.038	+	0.28	–	0.001	–	< 0.001	+	< 0.001	–	< 0.001	+	0.003
EC-EARTH- RCA4	–	0.0001	–	0.46	–	0.85	–	0.27	–	< 0.001	–	< 0.001	–	0.0026	+	0.18
MIROC5- RCA4	+	0.021	+	< 0.001	–	< 0.001	–	0.001	–	< 0.001	–	0.17	–	< 0.001	+	0.6
MPI-ESM-LR- RCA4	–	< 0.001	+	< 0.001	+	0.043	+	0.001	–	< 0.001	–	0.33	+	0.68	–	< 0.001
NCC-NorESM1- RCA4	–	0.029	–	0.62	–	< 0.001	–	0.057	+	< 0.001	+	0.14	–	< 0.001	+	0.003
NOAA/GFDL-ESM2M- RCA4	+	< 0.001	–	< 0.001	–	< 0.001	+	0.013	–	0.87	+	0.44	–	0.01	–	< 0.001

Table 9 | Same as Table 4 but for evapotranspiration**Evapotranspiration****1981–2000**

	January		July		January		July	
	T	p-value	T	p-value	T	p-value	T	p-value

Simulated from observation

+

0.03

-

0.037**RCP 4.5****2020–2039****2040–2059****2060–2079****2080–2099**

	January		July		January		July		January		July	
	T	p-value	T	p-value	T	p-value	T	p-value	T	p-value	T	p-value

EC-EARTH- CCLM4-8-17

-

0.007

-

0.001

-

< 0.001

-

< 0.001

-

0.8

-

< 0.001

-

0.004

-

< 0.001

IPSL-CM5A-MR- RCA4

-

< 0.001

-

< 0.001

-

0.19

+

0.58

+

0.01

-

0.06

-

0.01

CCCma-CanESM2- RCA4

-

0.17

-

< 0.001

+

< 0.001

-

0.9

-

< 0.001

+

0.05

+

0.05

+

0.021

CNRM-CM5- CCLM4-8-17

+

< 0.001

+

< 0.001

+

0.9

-

0.44

+

< 0.001

+

< 0.001

+

0.02

+

0.03

CNRM-CM5- RCA4

+

0.8

+

< 0.001

-

0.02

+

0.14

-

0.9

-

0.03

-

0.12

-

0.58

EC-EARTH- RCA4

+

0.6

-

< 0.001

-

< 0.001

-

0.013

+

< 0.001

-

0.18

-

< 0.001

-

0.03

MIROC5- RCA4

+

< 0.001

-

0.1

-

< 0.001

+

0.09

+

0.05

-

< 0.001

-

0.63

+

< 0.001

MPI-ESM-LR- RCA4

+

0.1

-

0.5

+

0.11

+

< 0.001

+

< 0.001

+

0.29

-

0.21

+

< 0.001

NCC-NorESM1- RCA4

-

< 0.001

-

0.01

+

0.29

-

< 0.001

-

0.02

+

0.03

+

0.16

-

0.026

NOAA/GFDL-ESM2M- RCA4

-

< 0.001

-

0.9

-

< 0.001

-

< 0.001

+

0.22

+

< 0.001

-

< 0.001

-

< 0.001**RCP 8.5****2020–2039****2040–2059****2060–2079****2080–2099**

	January		July		January		July		January		July	
	T	p-value	T	p-value	T	p-value	T	p-value	T	p-value	T	p-value

EC-EARTH- CCLM4-8-17

+

0.9

+

< 0.001

+

0.054

-

0.48

-

< 0.001

-

0.75

-

< 0.001

+

0.006

IPSL-CM5A-MR- RCA4

-

< 0.001

+

0.73

-

< 0.001

-

0.14

-

< 0.001

-

0.043

+

< 0.001

-

< 0.001

CCCma-CanESM2- RCA4

+

< 0.001

+

0.014

+

0.45

-

0.036

-

0.45

-

< 0.001

-

< 0.001

-

< 0.001

CNRM-CM5- CCLM4-8-17

-

0.0011

-

0.01

-

0.032

+

0.011

+

< 0.001

-

< 0.001

-

< 0.001

+

0.61

CNRM-CM5- RCA4

-

< 0.001

-

< 0.001

-

0.021

+

0.006

-

< 0.001

+

< 0.001

-

< 0.001

+

0.9

EC-EARTH- RCA4

+

0.006

+

0.13

-

0.9

+

0.63

-

< 0.001

-

< 0.001

-

0.035

+

0.3

MIROC5- RCA4

+

0.9

+

< 0.001

-

0.032

-

< 0.001

-

< 0.001

-

< 0.001

-

< 0.001

-

0.05

MPI-ESM-LR- RCA4

-

< 0.001

+

< 0.001

+

< 0.001

+

0.0004

-

0.006

-

0.0002

+

< 0.001

-

< 0.001

NCC-NorESM1- RCA4

+

0.033

-

0.052

-

< 0.001

-

< 0.001

+

0.015

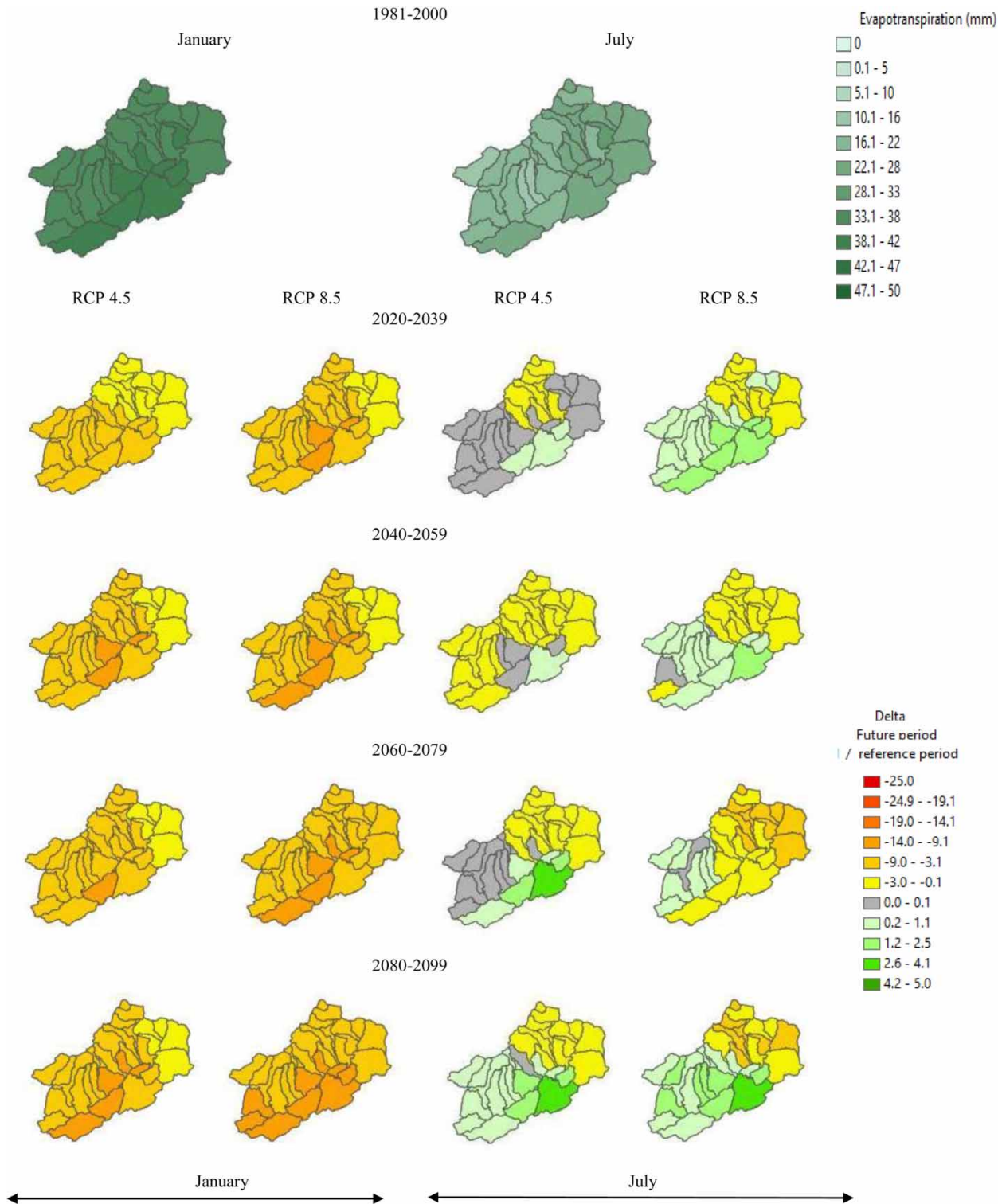


Figure 9 | Evapotranspiration during the reference period (1981–2000) and absolute variations for the periods (2020–2039, 2040–2059, 2060–2079, and 2080–2099) at monthly scale for January and July.

During the future period, our result is marked by a decline in precipitation in January to -44% under RCP 8.5. Brouziyne *et al.* (2018) also mention that the month mostly affected by climate change, in the future, is January with a reduction of precipitation reaching -49% under RCP 8.5 in the R'dom watershed (Morocco) near the Tafna basin. Zeroual *et al.* (2018) also confirm this decrease using RCMs of the CORDEX-Africa project, which highlights the aridification effect on hydrology. However, the increase in precipitation in July ($+30\%$) is also estimated by Taibi *et al.* (2017) for northern Algeria by the RCMs of the ENSEMBLE project and Hadour *et al.* (2020) and Brouziyne *et al.* (2018), using RCMs of the CORDEX project in northwestern Algeria and northern Morocco, respectively. On an annual scale, IPCC (2013), Jacob *et al.* (2014), Solomon *et al.* (2007), and Trambly *et al.* (2013) estimate a decrease in precipitation, reaching -30% under RCP 4.5 and more significant under RCP 8.5.

The Mann–Kendall test indicating the significant trends of decrease for the climate models are marked in the two last periods (2060–2079 and 2080–2099).

The tendency of the precipitation decrease in the rainy months in the future period, from November to March (Supplementary material, Figures S1 and S2) is similar to that of January. At the same time, the overestimation of precipitation shown in summer (Supplementary material, Figures S1 and S2) indicates an increase in the months of July, August, and September and that affects all of the components in the same months. These tendencies imply that January and July are representative of the rainy months (November to May) and the dry months (June to October).

In the future period, the decrease in precipitation has an impact on hydrological components. The precipitation decreasing trends directly lead to decreasing surface flow (between -20% and -48%) on the sub-basins of the Tafna watershed and decrease of the river discharge (between -42 and -54%), under RCPs 4.5 and 8.5. The tendency of decrease of the *river discharge* is also marked, for winter around -50% to -60% on average in the eastern part of the Tafna basin, in the study by Hadour *et al.* (2020). However, in July, the tendency is negligible in the future period, and this is due to the interception of the precipitation in the canopy storage (Neitsch *et al.* 2005). Therefore, this water is retained in the soil and made available for evapotranspiration. Under the two emission

scenarios RCP 4.5 and 8.5 the increase of river discharge and surface flow starts to appear in August and September (Supplementary material, Figures S3–S6) while the increase in precipitation starts in July, which implies these two months (August and September) are compensated by July. The tendency mentioned in January and July in the Tafna basin is also reported by Trambly *et al.* (2013) in the Moroccan region (R'dom basin) near the Tafna basin.

On the other hand, the lateral flow (subsurface flow) is also impacted by the decrease of precipitation and presents a considerable decrease in January around -37% and a less significant decrease in July. However, the decrease is more important in the months from February to April and is considered similar to January. An increase of the lateral flow appears after July, precisely in August, September, and October (Supplementary material, Figures S7 and S8). This increase is due to the hypothesis that the excess of water in the soil is subject to lateral movements (Grusson 2016), which are compensated during July.

The decrease of soil water availability (to -41%) and the temperature increase leads to a decrease of evapotranspiration as observed in January. Although evapotranspiration increases with temperature (Blanco-Gómez *et al.* 2019; Saddique *et al.* 2019; Dakhlaoui *et al.* 2020), the precipitation factor is primordial. We can confirm the decrease in evapotranspiration influenced by the decrease of precipitation (in January) and, therefore, the decrease of the soil water available. Bucak *et al.* (2017), Grusson *et al.* (2018), and Ertürk *et al.* (2014) also explain the decrease of evapotranspiration due to the low level of soil water availability caused by the decrease of precipitation and increase of temperature. Regarding the study by Zittis *et al.* (2019), the slight precipitation increase obtained in July for the future period affects the evapotranspiration by a small increase in the same month.

The dependence of the evapotranspiration on the soil water availability is confirmed during warm months in July and August (Supplementary material, Figures S9–S12). The increase of the evapotranspiration appears in August after the appearance of the increase in soil water availability in July.

The spatial distribution of water cycle effects is related to the surrounding areas. The effects of climate change on the major SWAT component outputs (surface flow, river discharge, precipitation, evapotranspiration, and soil water available) are visibly marked by the decrease, in the future

period, in the southern part of the basin, close to the Sahara where the temperature is higher and precipitation is lower. The distribution of the subsurface flow depends on the spatial distribution of slope classes in the basin, which implies the proportional relation between the subsurface flow and the slope classes, promoting more lateral flow during the reference period. That implies a visible change resulting in a decrease of surface flow in these areas of slopes. The decrease of the river discharge could cause an imbalance between urban water demand and supply, particularly the drinking water, which represents the major proportion. The decrease of the soil water available and the evapotranspiration might cause periods of drought, and increase the irrigation demand.

In the future period, the SWAT component outputs (precipitation, runoff, lateral flow, and evapotranspiration) are not so affected by the decrease in July, because during the reference period, their values are already quite low, and the climate models overestimate the precipitation in summer, particularly in July and August. That could lead to taking into consideration the uncertainty of the overestimation of the precipitation from climate models during the dry months in the Tafna basin, and the northwestern region of Algeria (Taibi *et al.* 2017; Hadour *et al.* 2020).

The last two periods, 2060–2079 and 2080–2099, are more impacted than the first ones, 2020–2039 and 2040–2059. In line with the study of Zittis *et al.* (2019), the precipitation in the southern part of the Mediterranean region is projected to decrease during all seasons. This decrease might be similar over North Africa for precipitation, soil water content, runoff, and evapotranspiration (Bates *et al.* 2008). In the fifth Report of the IPCC (AR5 Climate Change 2013), the precipitation has also been expected to decrease during winter with –30% in northwestern Africa, under RCP 8.5 during 2081–2100. At the annual scale, the study by Zittis *et al.* (2019) reported a decrease of –30% and –40% in precipitation, under RCP 4.5 and 8.5, respectively, in northwestern Africa. The soil moisture, runoff, and evaporation have the same tendency of decrease in northwestern Africa, which strengthens the results presented in the Fifth Report of the IPCC (IPCC Working Group I *et al.* 2013), and align our results in the same order of recent studies on the North Africa region.

The tendency of decrease of the SWAT components (river discharge, evapotranspiration, soil water available,

etc.) evaluated in this study might include an increase of drought periods, implying an increase in water irrigation demand, and water drinking demand, under the condition of the demographic evolution, which is estimated to increase until 2040 (Lakehal 2019), still increasing over the 21st century. That could cause strong tensions around the water resources and their uses in the studied region.

CONCLUSION

To understand the spatial and temporal changes in hydrological water balance in the future, the SWAT model has been implemented and forced by unbiased regional climate models for the semi-arid Tafna basin (northwest Algeria), as an example of a watershed particularly vulnerable to droughts in North Africa. The present study displays spatial trends of water components (surface flow, subsurface flow, soil water content, etc.) for two months (January and July), and under two pathway scenarios (RCP 4.5 and 8.5). These months are representative of the dry (summer) and wet (winter) seasons and are the months most impacted by climate change.

From these results, we conclude that the SWAT model has a good performance on the semi-arid Tafna basin.

From this study, we conclude that the decline of the precipitation impacts the hydrological water balance, from the river discharge to the evapotranspiration going through the lateral flow and soil water content of the Tafna basin. This decrease is more visible in the wet (January) than dry (July) seasons. These months, January and July, are representative of the rest of the months November to March and April to October, respectively.

The decline in precipitation affects all of the hydrological water components treated in this study by the decline, especially in wet months (from November to May), of the river discharge, the evapotranspiration, the soil water available, and subsurface flow. This decline is more significantly marked in the last periods 2060–2079 and 2080–2099 than the first two periods 2020–2039 and 2040–2059. The projected precipitation marks a slight increase during the summer, over the future period, when the precipitation is considered negligible during the reference period. The projected SWAT components' outputs have the same tendency of a slight increase in the Tafna basin.

Finally, the future changes of the hydrological components obtained with RCP 8.5 appear more visible than with RCP 4.5, throughout the future period. These changes are marked by the decrease of water resources in the studied basin, by the decrease of water cycle components. That could induce an imbalance between the demand and supply of water resources, in irrigation and urban domains in northwestern Algeria.

ACKNOWLEDGEMENTS

The authors wish to thank Algerian institutions (Agence Nationale des Ressources Hydriques, Office National de Météorologie) for providing data series; Amina Mami's stay in France was made possible thanks to a scholarship from 'National Exceptional Program' (PNE-2017) awarded by the Ministry of Higher Education and Scientific Research of Algeria. The laboratory of ecology environmental is gratefully acknowledged for its support of this research project and Eleni Katragkou from the CORDEX Group. Amina Mami, Djilali Yebdri, Sabine Sauvage, and José Miguel Sánchez-Pérez conceived and designed the experiments; Amina Mami performed the experiments; Amina Mami, Djilali Yebdri, Sabine Sauvage, Mélanie Raimonet, and José Miguel Sánchez-Pérez analyzed the results; Amina Mami, Djilali Yebdri, Sabine Sauvage, Mélanie Raimonet, and José Miguel Sánchez-Pérez wrote the paper.

CONFLICT OF INTEREST

The authors declare no conflict of interest.

DATA AVAILABILITY STATEMENT

All relevant data are included in the paper or its Supplementary Information.

REFERENCES

- Abbaspour, K. C. 2007 *SWAT-CUP: SWAT Calibration and Uncertainty Programs – A User Manual*. Swiss Federal Institute of Aquatic Science and Technology, Dübendorf, Switzerland.
- Abbaspour, K. C., Johnson, C. A. & van Genuchten, M. T. 2004 *Estimating uncertain flow and transport parameters using a sequential uncertainty fitting procedure*. *Vadose Zone J.* **3**, 1340–1352. <https://doi.org/10.2136/vzj2004.1340>.
- Abbott, M. B., Bathurst, J. C., Cunge, J. A., O'Connell, P. E. & Rasmussen, J. 1986 *An introduction to the European hydrological system – système hydrologique Européen, 'SHE', 1: history and philosophy of a physically-based, distributed modelling system*. *J. Hydrol.* **87**, 45–59. [https://doi.org/10.1016/0022-1694\(86\)90114-9](https://doi.org/10.1016/0022-1694(86)90114-9).
- Agence Nationale des Ressources Hydriques 1981 *Daily Data Flow in the North of Algeria*. Available from: <http://www.anrh.dz/>
- ANBT 2015 *Agence Nationale des Barrages et Transferts*. Available from: http://197.112.0.211/soudoud-dzair/?action=contact_generale
- AR4 2007 *AR4 Climate Change 2007: Synthesis Report – IPCC [WWW Document]*. Available from: <https://www.ipcc.ch/report/ar4/syr/> (accessed 1.6.20).
- AR5 2013 *AR5 Climate Change 2013: The Physical Science Basis – IPCC [WWW Document]*, 2013. Available from: <https://www.ipcc.ch/report/ar5/wg1/> (accessed 2.11.19).
- Arnell, N. W. 1999 *Climate change and global water resources*. *Global Environ. Change* **9**, S31–S49. [https://doi.org/10.1016/S0959-3780\(99\)00017-5](https://doi.org/10.1016/S0959-3780(99)00017-5).
- Arnell, N. W., Hudson, D. A. & Jones, R. G. 2003 *Climate change scenarios from a regional climate model: estimating change in runoff in southern Africa*. *J. Geophys. Res. Atmos.* **108** (D16). <https://doi.org/10.1029/2002JD002782>.
- Arnold, J. G., Srinivasan, R., Muttiah, R. S. & Williams, J. R. 1998 *Large area hydrologic modeling and assessment part I: model development*. *J. Am. Water Resour. Assoc.* **34**, 73–89. <https://doi.org/10.1111/j.1752-1688.1998.tb05961.x>.
- Arnold, J. G., Srinivasan, R., Gassman, P. W., White, M. J., Abbaspour, K. C., Santhi, C., Harmel, R. D., van Griensven, A. & Moriasi, D. N. 2012 *SWAT: model use, calibration, and validation*. *Am. Soc. Agric. Biol. Eng.* **55** (4), 1491–1508.
- Bates, B., Kundzewicz, Z. W., Wu, S. & Palutikof, J. 2008 *Climate Change and Water. IPCC Technical Paper 6*. Intergovernmental Panel on Climate Change, Geneva, Switzerland.
- Beven, K., Calver, A. & Morris, E. M. 1987 *The Institute of Hydrology Distributed Model*. Institute of Hydrology, Wallingford, UK. Available from: <http://nora.nerc.ac.uk/id/eprint/5977/> (accessed 12.3.19).
- Blanco-Gómez, P., Jimeno-Sáez, P., Senent-Aparicio, J. & Pérez-Sánchez, J. 2019 *Impact of climate change on water balance components and droughts in the Guajoyo River Basin (El Salvador)*. *Water* **11**, 2360. <https://doi.org/10.3390/w11112360>.
- Block, P. J., Filho, F. A. S., Sun, L. & Kwon, H.-H. 2009 *A streamflow forecasting framework using multiple climate and hydrological models*. *J. Am. Water Resour. Assoc.* **45**, 828–843. <https://doi.org/10.1111/j.1752-1688.2009.00327.x>.
- Bouraoui, F., Benabdallah, S., Jrad, A. & Bidoglio, G. 2005 *Application of the SWAT model on the Medjerda river basin*

- (Tunisia). *Phys. Chem. Earth Parts ABC, Assessment of Anthropogenic Impacts on Water Quality* **30**, 497–507. <https://doi.org/10.1016/j.pce.2005.07.004>.
- Brouziyne, Y., Abouabdillah, A., Hirich, A., Bouabid, R., Zaaboul, R. & Benaabidate, L. 2018 **Modeling sustainable adaptation strategies toward a climate-smart agriculture in a Mediterranean watershed under projected climate change scenarios**. *J. Mater. Environ. Sci.* **9**, 154–163. <https://doi.org/10.26872/jmes.2018.9.1.16>.
- Bucak, T., Trolle, D., Andersen, H. E., Thodsen, H., Erdoğan, Ş., Levi, E. E., Filiz, N., Jeppesen, E. & Beklioglu, M. 2017 **Future water availability in the largest freshwater Mediterranean lake is at great risk as evidenced from simulations with the SWAT model**. *Sci. Total Environ.* **581–582**, 413–425. <https://doi.org/10.1016/j.scitotenv.2016.12.149>.
- Burek, P., Satoh, Y., Kahil, T., Tang, T., Greve, P., Smilovic, M., Guillaume, L. & Wada, Y. 2019 **Development of the community water model (CWatM v1.04): a high-resolution hydrological model for global and regional assessment of integrated water resources management**. *Geosci. Model Dev. Discuss.* **13** (7), 3267–3298. <https://doi.org/10.5194/gmd-2019-214>.
- Calanca, P., Roesch, A., Jasper, K. & Wild, M. 2006 **Global warming and the summertime evapotranspiration regime of the alpine region**. *Clim. Change* **79**, 65–78. <https://doi.org/10.1007/s10584-006-9103-9>.
- Chen, J., Brissette, F. P. & Leconte, R. 2011 **Uncertainty of downscaling method in quantifying the impact of climate change on hydrology**. *J. Hydrol.* **401**, 190–202. <https://doi.org/10.1016/j.jhydrol.2011.02.020>.
- CORDEX Data Search | CORDEX | ESGF-CoG [WWW Document], n.d. Available from: <https://esg-dn1.nsc.liu.se/search/cordex/> (accessed 10.30.2018).
- Dakhlou, H., Seibert, J. & Hakala, K. 2020 **Sensitivity of discharge projections to potential evapotranspiration estimation in Northern Tunisia**. *Reg. Environ. Change* **20** (2), 34. <https://doi.org/10.1007/s10113-020-01615-8>.
- Ertürk, A., Ekdal, A., Gürel, M., Karakaya, N., Guzel, C. & Gönenç, E. 2014 **Evaluating the impact of climate change on groundwater resources in a small Mediterranean watershed**. *Sci. Total Environ.* **499**, 437–447. <https://doi.org/10.1016/j.scitotenv.2014.07.001>.
- Fang, G. H., Yang, J., Chen, Y. N. & Zammit, C. 2015 **Comparing bias correction methods in downscaling meteorological variables for a hydrologic impact study in an arid area in China**. *Hydrol. Earth Syst. Sci.* **19**, 2547–2559. <https://doi.org/10.5194/hess-19-2547-2015>.
- Gassman, P. W., Sadeghi, A. M. & Srinivasan, R. 2014 **Applications of the SWAT model special section: overview and insights**. *J. Environ. Qual.* **43**, 1–8. <https://doi.org/10.2134/jeq2013.11.0466>.
- Gevaert, A., Veldkamp, T. & Ward, P. 2018 **The effect of climate type on timescales of drought propagation in an ensemble of global hydrological models**. *Hydrol. Earth Syst. Sci.* **22**, 4649–4665.
- Green, T. R. 2016 **Linking climate change and groundwater**. In: *Integrated Groundwater Management: Concepts, Approaches and Challenges* (A. J. Jakeman, O. Barreteau, R. J. Hunt, J.-D. Rinaudo & A. Ross, eds). Springer International Publishing, Cham, Switzerland, pp. 97–141. https://doi.org/10.1007/978-3-319-23576-9_5.
- Grusson, Y. 2016 *Modeling of the Hydroclimatic Evolution of Flows and Stocks of Green Water and Blue Water in the Garonne Watershed*. PhD Thesis, Université Laval Québec, Canada/INP Toulouse, France.
- Grusson, Y., Anctil, F. & Sánchez Pérez, J. M. 2018 **Coevolution of hydrological cycle components under climate change: the case of the Garonne River in France**. *Water-MDPI* **10** (12), 1870. <https://doi.org/10.3390/w10121870>.
- Hadour, A., Mahé, G. & Meddi, M. 2020 **Watershed based hydrological evolution under climate change effect: an example from North Western Algeria**. *J. Hydrol. Reg. Stud.* **28**, 100671. <https://doi.org/10.1016/j.ejrh.2020.100671>.
- IPCC 2013 *Climate Change 2013: The Physical Science Basis*. Contribution of Working Group I to the Fifth Assessment Report of the Intergovernmental Panel on Climate Change (T. F. Stocker, D. Qin, G.-K. Plattner, M. Tignor, S. K. Allen, J. Boschung, A. Nauels, Y. Xia, V. Bex and P. M. Midgley (eds.)). Cambridge University Press, Cambridge, UK and New York, NY, USA, 1535 pp.
- Jacob, D., Petersen, J., Eggert, B., Alias, A., Christensen, O. B., Bouwer, L. M., Braun, A., Colette, A., Déqué, M., Georgievski, G., Georgopoulou, E., Gobiet, A., Menut, L., Nikulin, G., Haensler, A., Hempelmann, N., Jones, C., Keuler, K., Kovats, S., Kröner, N., Kotlarski, S., Kriegsmann, A., Martin, E., van Meijgaard, E., Moseley, C., Pfeifer, S., Preuschmann, S., Radermacher, C., Radtke, K., Rechid, D., Rounsevell, M., Samuelsson, P., Somot, S., Soussana, J.-F., Teichmann, C., Valentini, R., Vautard, R., Weber, B. & Yiou, P. 2014 **EURO-CORDEX: new high-resolution climate change projections for European impact research**. *Reg. Environ. Change* **14**, 563–578. <https://doi.org/10.1007/s10113-013-0499-2>.
- Jianwen, B., Zhenyao, S. & Tiezhu, Y. 2017 **A comparison of single- and multi-site calibration and validation: a case study of SWAT in the Miyun Reservoir watershed, China**. *Front. Earth Sci.* **11**, 592–600. <https://doi.org/10.1007/s11707-017-0656-x>.
- Jin, H., Zhu, Q., Zhao, X. & Zhang, Y. 2016 **Simulation and prediction of climate variability and assessment of the response of water resources in a typical watershed in China**. *Water* **8**, 490. <https://doi.org/10.3390/w8110490>.
- Jung, M., Reichstein, M., Ciais, P., Seneviratne, S. I., Sheffield, J., Goulden, M. L., Bonan, G., Cescatti, A., Chen, J., Jiu, R. d., Dolman, A. J., Eugster, W., Gerten, D., Gianelle, D., Gobron, N., Heinke, J., Kimball, J., Law, B. E., Montagnani, L., Mu, Q., Mueller, B., Oleson, K., Papale, D., Richardson, A. D., Rouspard, O., Running, S., Tomelleri, E., Viovy, N., Weber, U., Williams, C., Wood, E., Zaehle, S. & Zhang, K. 2010 **Recent decline in the global land evapotranspiration trend due to limited moisture supply**. *Nature* **467**, 951–954. <https://doi.org/10.1038/nature09396>.

- Knippertz, P., Christoph, M. & Speth, P. 2003 Long-term precipitation variability in Morocco and the link to the large-scale circulation in recent and future climates. *Meteorol. Atmos. Phys.* **83**, 67–88. <https://doi.org/10.1007/s00703-002-0561-y>.
- Knoben, W. J. M., Freer, J. E. & Woods, R. A. 2019 Technical note: inherent benchmark or not? comparing Nash–Sutcliffe and Kling–Gupta efficiency scores. *Hydrol. Earth Syst. Sci.* **23**, 4323–4331. <https://doi.org/10.5194/hess-23-4323-2019>.
- Kouwen, N., Soulis, E. D., Pietroniro, A. & Donald, J. 1993 Grouped response units for distributed hydrologic modeling. *J. Water Resour. Plan. Manage.* **119**. [https://doi.org/10.1061/\(ASCE\)0733-9496\(1993\)119:3\(289\)](https://doi.org/10.1061/(ASCE)0733-9496(1993)119:3(289))
- Kundzewicz, Z. W. & Doll, P. 2009 Will groundwater ease freshwater stress under climate change? *Hydrol. Sci. J.* **54**, 665–675. <https://doi.org/10.1623/hysj.54.4.665>.
- Lakehal, A. 2019 *Demographie Algerienne* 2008. Office of National Statistics (Algeria) 32.
- Leta, O. T., van Griensven, A. & Bauwens, W. 2017 Effect of single and multisite calibration techniques on the parameter estimation, performance, and output of a SWAT model of a spatially heterogeneous catchment. *J. Hydrol. Eng.* **22** (3). [https://doi.org/10.1061/\(ASCE\)HE.1943-5584.0001471](https://doi.org/10.1061/(ASCE)HE.1943-5584.0001471)
- Liang, X., Lettenmaier, D. P., Wood, E. F. & Burges, S. J. 1994 A simple hydrologically based model of land surface water and energy fluxes for general circulation models. *J. Geophys. Res.* **99**, 14415–14428. <https://doi.org/10.1029/94JD00483>.
- Lin, B., Chen, X., Yao, H., Chen, Y., Liu, M., Gao, L. & James, A. 2015 Analyses of landuse change impacts on catchment runoff using different time indicators based on SWAT model. *Ecol. Indic.* **58**, 55–63. <https://doi.org/10.1016/j.ecolind.2015.05.031>.
- Mami, A., Raimonet, M., Yebdri, D., Sauvage, S., Zettam, A. & Sanchez-Perez, J.-M. 2021 Future climatic and hydrologic changes estimated by bias-adjusted regional climate model outputs of the Cordex-Africa project: case of the Tafna basin (North-Western Africa). *Int. J. Global Warm.* **23** (1), 58–90.
- Manabe, S., Milly, P. C. D. & Wetherald, R. 2004 Simulated long-term changes in river discharge and soil moisture due to global warming/Simulations à long terme de changements d'écoulement fluvial et d'humidité du sol causés par le réchauffement global. *Hydrol. Sci. J.* **49**, 642. <https://doi.org/10.1623/hysj.49.4.625.54429>.
- Mann, H. B. 1945 Non parametric tests against trend. *Econom. Soc.* **13**, 245–259. <https://doi.org/DOI:10.2307/1907187>.
- Meddi, M. & Hubert, P. 2003 Impact of the modification of the rainfall regime on the water resources of northwest Algeria. In *Proceedings of an International Symposium*, April 2003, Montpellier, France. IAHS Publ. no. 278, pp. 229–235.
- Meddi, M., Assani, A. A. & Meddi, H. 2010 Temporal variability of annual rainfall in the Macta and Tafna catchments, Northwestern Algeria. *Water Resour. Manage.* **24**, 3817–3833. <https://doi.org/10.1007/s11269-010-9635-7>.
- Meddi, M., Toumi, S. & Assani, A. A. 2016 Spatial and temporal variability of the rainfall erosivity factor in Northern Algeria. *Arab. J. Geosci.* **9**, 282. <https://doi.org/10.1007/s12517-015-2303-8>.
- Molina-Navarro, E., Trolle, D., Martínez-Pérez, S., Sastre-Merlín, A. & Jeppesen, E. 2014 Hydrological and water quality impact assessment of a Mediterranean limno-reservoir under climate change and land use management scenarios. *J. Hydrol.* **509**, 354–366. <https://doi.org/10.1016/j.jhydrol.2013.11.053>.
- Moriasi, D. N., Steiner, J. L. & Arnold, J. G. 2011 Sediment measurement and transport modeling: impact of Riparian and filter strip buffers. *J. Environ. Qual.* **40**, 807–814. <https://doi.org/10.2134/jeq2010.0066>.
- Nash, J. E. & Sutcliffe, J. V. 1970 River flow forecasting through conceptual models part I – a discussion of principles. *J. Hydrol.* **10**, 282–290. [https://doi.org/10.1016/0022-1694\(70\)90255-6](https://doi.org/10.1016/0022-1694(70)90255-6).
- National Agency of Hydrologic Resources (ANRH) 2003a *Map of Potential Evapotranspiration in the North of Algeria*. Available from: <http://www.anrh.dz/cartevapo.htm>
- National Agency of Hydrologic Resources (ANRH) 2003b *Map of Annual Rainfall in the North of Algeria*. Available from: <http://www.anrh.dz/pluvio.htm>
- National Agency of Hydrologic Resources (ANRH) 2003c *Map of Average Annual Runoff in the North of Algeria*. Available from: <http://www.anrh.dz/cartecoulement.htm>
- Naumann, G., Alfieri, L., Wyser, K., Mentaschi, L., Betts, R. A., Carrao, H., Spinoni, J., Vogt, J. & Feyen, L. 2018 Global changes in drought conditions under different levels of warming. *Geophys. Res. Lett.* **45**, 3285–3296. <https://doi.org/10.1002/2017GL076521>.
- Neitsch, S. L., Arnold, J. G., Kiniry, J. R. & Williams, J. R. 2005 *Soil and Water Assessment Tool Theoretical Documentation*. Texas Water Resources Institute Technical Report No. 494. Texas A&M University System, College Station, TX, USA.
- Nerantzaki, S. D., Giannakis, G. V., Efstathiou, D., Nikolaidis, N. P., Sibtheros, I. A., Karatzas, G. P. & Zacharias, I. 2015 Modeling suspended sediment transport and assessing the impacts of climate change in a karstic Mediterranean watershed. *Sci. Total Environ.* **538**, 288–297. <https://doi.org/10.1016/j.scitotenv.2015.07.092>.
- Niraula, R., Norman, L. M., Meixner, T. & Callegary, J. B. 2012 Multi-gauge calibration for modeling the semi-arid Santa Cruz watershed in Arizona-Mexico border area using SWAT. *Air Soil Water Res.* **5**, 41–57. <https://doi.org/10.4137/ASWR.S9410>.
- Noori, N. & Kalin, L. 2016 Coupling SWAT and ANN models for enhanced daily streamflow prediction. *J. Hydrol.* **533**, 141–151. <https://doi.org/10.1016/j.jhydrol.2015.11.050>.
- Price, R. 2017 *Climate Change and Stability in North Africa. K4D Helpdesk Report No. 242*. Institute of Development Studies, Brighton, UK.
- Rathjens, H., Bieger, K., Srinivasan, R., Chaubey, I. & Arnold, J. G. 2016 *CMhyd User Manual*. Available from: https://swat.tamu.edu/media/115265/bias_cor_man.pdf
- Saddique, N., Usman, M. & Bernhofer, C. 2019 Simulating the impact of climate change on the hydrological regimes of a sparsely gauged mountainous basin, Northern Pakistan. *Water* **11**, 2141. <https://doi.org/10.3390/w11102141>.

- Santos, C. A. S., Rocha, F. A., Ramos, T. B., Alves, L. M., Mateus, M., de Oliveira, R. P. & Neves, R. 2019 Using a hydrologic model to assess the performance of regional climate models in a semi-arid watershed in Brazil. *Water* **11**, 170. <https://doi.org/10.3390/w11010170>.
- Schilling, J., Freier, K. P., Hertig, E. & Scheffran, J. 2012 Climate change, vulnerability and adaptation in North Africa with focus on Morocco. *Agric. Ecosyst. Environ.* **156**, 12–26. <http://dx.doi.org/10.1016/j.agee.2012.04.021>.
- Seif-Ennasr, M., Zaaboul, R., Hirich, A., Caroletti, G. N., Bouchaou, L., El Morjani, Z. E. A., Beraaouz, E. H., McDonnell, R. A. & Choukr-Allah, R. 2016 Climate change and adaptive water management measures in Chtouka Aït Baha region (Morocco). *Sci. Total Environ.* **573**, 862–875. <https://doi.org/10.1016/j.scitotenv.2016.08.170>.
- Sellami, H., Benabdallah, S., La Jeunesse, I. & Vanclooster, M. 2016 Quantifying hydrological responses of small Mediterranean catchments under climate change projections. *Sci. Total Environ.* **543**, 924–936. <https://doi.org/10.1016/j.scitotenv.2015.07.006>.
- Shrestha, M. K., Recknagel, F., Frizenschaf, J. & Meyer, W. 2016 Assessing SWAT models based on single and multi-site calibration for the simulation of flow and nutrient loads in the semi-arid Onkaparinga catchment in South Australia. *Agric. Water Manage.* **175**, 61–71. <https://doi.org/10.1016/j.agwat.2016.02.009>.
- Singh, A. & Gosain, A. K. 2011 Climate-change impact assessment using GIS-based hydrological modelling. *Water Int.* **36**, 386–397. <https://doi.org/10.1080/02508060.2011.586761>.
- Solomon, S., Qin, D. & Manning, M. 2007 *Intergovernmental Panel on Climate Change. Climate Change 2007: the Physical Science Basis: Contribution of Working Group I to the Fourth Assessment Report of the Intergovernmental Panel on Climate Change*. Cambridge University Press, Cambridge, UK and New York, USA.
- Taibi, S., Meddi, M., Mahe, G. & Assani, A. 2017 Relationships between atmospheric circulation indices and rainfall in Northern Algeria and comparison of observed and RCM-generated rainfall. *Theor. Appl. Climatol.* **127**, 241–257. <https://doi.org/10.1007/s00704-015-1626-4>.
- Taylor, K. E., Stouffer, R. J. & Meehl, G. A. 2011 An overview of CMIP5 and the experiment design. *Bull. Am. Meteorol. Soc.* **93**, 485–498. <https://doi.org/10.1175/BAMS-D-11-00094.1>.
- Teutschbein, C. & Seibert, J. 2012 Bias correction of regional climate model simulations for hydrological climate-change impact studies: review and evaluation of different methods. *J. Hydrol.* **456–457**, 12–29. <https://doi.org/10.1016/j.jhydrol.2012.05.052>.
- Teutschbein, C. & Seibert, J. 2013 Is bias correction of regional climate model (RCM) simulations possible for non-stationary conditions? *Hydrol. Earth Syst. Sci.* **17**, 5061–5077. <https://doi.org/10.5194/hess-17-5061-2013>.
- Todini, E. 2007 Hydrological catchment modelling: past, present and future. *Hydrol. Earth Syst. Sci.* **11**, 468–482. <https://doi.org/10.5194/hess-11-468-2007>.
- Tramblay, Y., Ruelland, D., Somot, S., Bouaicha, R. & Servat, E. 2013 High-resolution Med-CORDEX regional climate model simulations for hydrological impact studies: a first evaluation of the ALADIN-Climate model in Morocco. *Hydrol. Earth Syst. Sci.* **17**, 3721–3739. <https://doi.org/10.5194/hess-17-3721-2013>.
- Verrot, L. & Destouni, G. 2016 Worldwide soil moisture changes driven by future hydro-climatic change scenarios. *Hydrol. Earth Syst. Sci. Discuss.* 1–26. <https://doi.org/10.5194/hess-2016-165>.
- Xoplaki, E. 2002 *Climate Variability Over the Mediterranean. Doctoral Dissertation*, Universität Bern, Switzerland.
- Yanjie, B., Yong, Z., Weihua, X. & Di, W. 2015 The Quantitative Research of Impact of Climate Change and Reservoir Operation on the runoff Based on Computer Simulation. In *2015 Seventh International Conference on Measuring Technology and Mechatronics Automation*, Nanchang, China. pp. 1249–1252. <https://doi.org/10.1109/ICMTMA.2015.304>.
- Yebdri, D. 2006 *Contribution to the Management of Surface Water Resources in the Tafna Watershed. PhD Thesis*, University of Science and Technology of Oran ‘Mohamed Boudiaf’, Oran, Algeria.
- Yebdri, D., Errih, M., Hamlet, A. & Tidjani, A. E.-B. 2007 The water resources management study of the wadi tafna basin (Algeria) using the SWAT model. *Afr. Water J.* **1**, 33–47.
- Yuan, Z. 2019 Impact of climate variability on blue and green water flows in the erhai lake basin of southwest China. *Water* **11** (3), 424. <https://doi.org/10.3390/w11030424>.
- Zeroual, A., Assani, A. A., Meddi, M. & Alkama, R. 2018 Assessment of climate change in Algeria from 1951 to 2098 using the Köppen–Geiger climate classification scheme. *Clim. Dyn.* **52**, 227–243. <https://doi.org/10.1007/s00382-018-4128-0>.
- Zettam, A., Taleb, A., Sauvage, S., Boithias, L., Belaidi, N. & Sánchez-Pérez, J. M. 2017 Modelling hydrology and sediment transport in a semi-arid and anthropized catchment using the SWAT model: the case of the Tafna River (Northwest Algeria). *Water* **9**, 216. <https://doi.org/10.3390/w9030216>.
- Zettam, A., Taleb, A., Sauvage, S., Boithias, L., Belaidi, N. & Sanchez-Perez, J. M. 2020 Applications of a SWAT model to evaluate the contribution of the Tafna catchment (north-West Africa) to the nitrate load entering the Mediterranean Sea. *Environ. Monit. Assess.* **192**, 510. <https://doi.org/10.1007/s10661-020-08482-0>.
- Zittis, G., Hadjinicolaou, P., Klangidou, M., Proestos, Y. & Lelieveld, J. 2019 A multi-model, multi-scenario, and multi-domain analysis of regional climate projections for the Mediterranean. *Reg. Environ. Change* **19**, 2621–2635. <https://doi.org/10.1007/s10113-019-01565-w>.